



HAL
open science

Open clusters in APOGEE and GALAH: Combining Gaia and ground-based spectroscopic surveys

R. Carrera, A. Bragaglia, T. Cantat-Gaudin, A. Vallenari, L. Balaguer-Núñez,
D. Bossini, L. Casamiquela, C. Jordi, R. Sordo, C. Soubiran

► **To cite this version:**

R. Carrera, A. Bragaglia, T. Cantat-Gaudin, A. Vallenari, L. Balaguer-Núñez, et al.. Open clusters in APOGEE and GALAH: Combining Gaia and ground-based spectroscopic surveys. *Astronomy and Astrophysics - A&A*, 2019, 623, pp.id.A80. 10.1051/0004-6361/201834546 . hal-02005344

HAL Id: hal-02005344

<https://hal.science/hal-02005344>

Submitted on 9 Jul 2022

HAL is a multi-disciplinary open access archive for the deposit and dissemination of scientific research documents, whether they are published or not. The documents may come from teaching and research institutions in France or abroad, or from public or private research centers.

L'archive ouverte pluridisciplinaire **HAL**, est destinée au dépôt et à la diffusion de documents scientifiques de niveau recherche, publiés ou non, émanant des établissements d'enseignement et de recherche français ou étrangers, des laboratoires publics ou privés.

Open clusters in APOGEE and GALAH

Combining *Gaia* and ground-based spectroscopic surveys[★]

R. Carrera¹, A. Bragaglia², T. Cantat-Gaudin³, A. Vallenari¹, L. Balaguer-Núñez³, D. Bossini¹, L. Casamiquela⁴,
C. Jordi³, R. Sordo¹, and C. Soubiran⁴

¹ INAF-Osservatorio Astronomico di Padova, vicolo dell'Osservatorio 5, 35122 Padova, Italy
e-mail: jimenez.carrera@inaf.it

² INAF-Osservatorio di Astrofisica e Scienza dello Spazio, via P. Gobetti 93/3, 40129 Bologna, Italy

³ Institut de Ciències del Cosmos, Universitat de Barcelona (IEEC-UB), Martí i Franquès 1, 08028 Barcelona, Spain

⁴ Laboratoire d'Astrophysique de Bordeaux, Univ. Bordeaux, CNRS, B18N, allée Geoffroy Saint-Hilaire, 33615 Pessac, France

Received 31 October 2018 / Accepted 26 January 2019

ABSTRACT

Context. Open clusters are ideal laboratories to investigate a variety of astrophysical topics, from the properties of the Galactic disc to stellar-evolution models. Knowing their metallicity and possibly detailed chemical abundances is therefore important. However, the number of systems with chemical abundances determined from high-resolution spectroscopy remains small.

Aims. Our aim is to increase the number of open clusters with radial velocities and chemical abundances determined from high-resolution spectroscopy using publicly available catalogues of surveys in combination with *Gaia* data.

Methods. Open cluster stars have been identified in the APOGEE and GALAH spectroscopic surveys by cross-matching their latest data releases with stars for which high-probability astrometric membership has been derived in many clusters on the basis of the *Gaia* second data release.

Results. Radial velocities were determined for 131 and 14 clusters from APOGEE and GALAH data, respectively. This is the first radial-velocity determination from high-resolution spectra for 16 systems. Iron abundances were obtained for 90 and 14 systems from APOGEE and GALAH samples, respectively. To our knowledge 66 of these clusters (57 in APOGEE and 9 in GALAH) do not have previous determinations in the literature. For 90 and 7 clusters in the APOGEE and GALAH samples, respectively, we also determined average abundances for Na, Mg, Al, Si, Ca, Cr, Mn, and Ni.

Key words. stars: abundances – open clusters and associations: general

1. Introduction

Open clusters (OCs) are groupings of between ten and a few thousand stars that share chemo-dynamical features with a common birth time and place. They are probably the only chemically homogeneous stellar populations (e.g. De Silva et al. 2007; Bovy 2016, but see also Liu et al. 2016). These systems play a fundamental role in our understanding of both individual and group stellar evolution allowing us to investigate a variety of astrophysical topics such as initial mass function, initial binary fraction, the creation of blue stragglers, mass loss, or atomic diffusion among others. Thanks to the fact that OCs cover a wide range of ages and are found everywhere in the Galactic disc, they have been widely used to trace both the disc chemistry, for example the disc metallicity gradient (e.g. Friel et al. 2002; Donati et al. 2015a; Jacobson et al. 2016; Netopil et al. 2016; Casamiquela et al. 2017), and its evolution with time (e.g. Andreuzzi et al. 2011; Carrera & Pancino 2011), and dynamics, for example individual orbits (e.g. Cantat-Gaudin et al. 2016; Reddy et al. 2016) or radial migration (e.g. Roškar et al. 2008; Anders et al. 2017).

A detailed characterisation of the chemical composition of the OCs is necessary to fully exploit their capabilities to address the topics described above. High-resolution spectroscopy ($R \geq 20\,000$) is the most direct way to obtain chemical abundances; however, for some OCs these studies have been limited to the determination of the iron content, widely known as metallicity¹. Moreover, this kind of analysis has been performed for slightly more than 100 objects (see e.g. the literature compilations by Carrera & Pancino 2011; Yong et al. 2012; Heiter et al. 2014; Donati et al. 2015a; Netopil et al. 2016), which is about 10% of the approximately 3000 known OCs according to the updated versions of the two most used OCs compilations by Dias et al. (2002, DAML) and Kharchenko et al. (2013, MWSC). The real cluster population is still largely unknown; not only do many of these 3000 objects need to be confirmed as real clusters (see e.g. Kos et al. 2018a; Cantat-Gaudin et al. 2018, for objects that are likely not clusters), but new clusters are being discovered thanks to surveys like the *Gaia* mission (see below).

The *Gaia* mission (Gaia Collaboration 2016) is revolutionising astronomy by providing a volume of unprecedented size of high-quality positions, parallaxes and proper motions. This is

[★] Full Table 2 and Appendix tables are only available at the CDS via anonymous ftp to cdsarc.u-strasbg.fr (130.79.128.5) or via <http://cdsarc.u-strasbg.fr/viz-bin/qcat?J/A+A/623/A80>

¹ There is some ambiguity in the use of the term “metallicity” in the literature. Together with the iron abundance, typically denoted as [Fe/H], the term metallicity is also used to refer to the overall abundance of all elements heavier than helium, written [M/H].

supplemented by very high-accuracy all-sky photometric measurements. Additionally, for the brightest stars *Gaia* is also providing radial velocities (RVs; Sartoretti et al. 2018) and in the future it will provide some information about their chemical composition (Bailer-Jones et al. 2013).

Complementation of the limited spectroscopic capabilities of *Gaia* is the motivation for several ongoing and forthcoming ground-based high-resolution spectroscopic surveys providing RVs and chemical abundances for more than 20 chemical species. Currently, the *Gaia*-ESO Survey (GES, Gilmore et al. 2012; Randich & Gilmore 2013) is the only high-resolution survey which has dedicated a significant fraction of time to targeting OCs. *Gaia*-ESO is providing a homogeneous set for about 80 clusters (see e.g. Jacobson et al. 2016; Randich et al. 2018, and references therein) observed extensively (100–1000 stars targeted in each of them). The other two high-resolution surveys with already published data, APOGEE (Apache Point Observatory Galactic Evolution Experiment; Majewski et al. 2017) and GALAH (Galactic Archaeology with HERMES; De Silva et al. 2015), do not have such a large and specific program on OCs, although they are targeting some of them, also for calibration purposes (see e.g. Donor et al. 2018; Kos et al. 2018b). Their latest data releases include about 277 000 (Holtzman et al. 2018) and 340 000 (Buder et al. 2018) stars, respectively.

This paper is the third of a series devoted to the study of OCs on the basis of *Gaia* data release 2 (DR2). In the first paper, membership probabilities for OCs were derived from the *Gaia* DR2 astrometric solutions (Cantat-Gaudin et al. 2018). In the second, the *Gaia* DR2 RVs were used to investigate the distribution of OCs in 6D space (Soubiran et al. 2018). The goal of this paper is to search for cluster stars hidden in both the APOGEE and GALAH catalogues² in order to increase the number of OCs with RVs and chemical abundances derived from high-resolution spectroscopy. To do so, we use the astrometric membership probabilities obtained by Cantat-Gaudin et al. (2018).

This paper is organised as follows. The observational material used in the paper is described in Sect. 2. The RVs are discussed in Sect. 3. The iron and other elements abundances are presented in Sects. 4 and 5, respectively. An example of the usefulness of the results obtained in previous sections in the investigation of radial and vertical chemical distributions of OCs in the Galactic disc is presented in Sect. 6. Finally, the main conclusions of this paper are discussed in Sect. 7.

2. The data

The *Gaia* DR2 provides a five-parameter astrometric solution (positions, proper motions μ_{α^*} , μ_{δ} , and parallaxes ϖ ; Lindegren et al. 2018) and magnitudes in three photometric bands (G , G_{BP} and G_{RP} ; Evans et al. 2018) for more than 1.3 billion sources (Gaia Collaboration 2018), plus RVs for more than 7 million stars (Katz et al. 2019). On the basis of *Gaia* DR2, Cantat-Gaudin et al. (2018) determined membership probabilities for stars in 1229 OCs, 60 of which are new clusters serendipitously discovered in the fields analysed. Because of the large uncertainties on the proper motion and parallax determinations for faint objects, the analysis was limited to stars with $G \leq 18$, corresponding to a typical uncertainty of 0.3 mas yr^{-1} and 0.15 mas in proper motion and parallax, respectively. To

assign the membership probabilities, p , these latter authors used the unsupervised photometric membership assignment in stellar clusters (UPMASK) developed by Krone-Martins & Moitinho (2014). We refer the reader to that paper for details on how the probabilities are assigned.

2.1. APOGEE

In the framework of the third and fourth phases of the Sloan Digital Sky Survey (Eisenstein et al. 2011; Blanton et al. 2017), APOGEE (Majewski et al. 2017) obtained $R \sim 22\,500$ spectra in the infrared H -band, $1.5\text{--}1.7 \mu\text{m}$. The fourteenth Data Release (DR14; Abolfathi et al. 2018; Holtzman et al. 2018) includes about 277 000 stars and provides RVs with a typical uncertainty of $\sim 0.1 \text{ km s}^{-1}$ (Nidever et al. 2015). Because APOGEE tries to observe each star at least three times, the RV uncertainty, called RV_{scatter} and defined as the scatter among the individual RV determinations, provides a possible indication of stellar binarity. Stellar parameters and abundances for 19 chemical species are determined with the APOGEE stellar parameter and chemical abundance pipeline (ASPCAP; García Pérez et al. 2016). Briefly, ASPCAP works in two steps: it first determines stellar parameters using a global fit over the entire spectral range by comparing the observed spectrum with a grid of synthetic spectra, and then it fits sequentially for individual elemental abundances over limited spectral windows using the initially derived parameters.

APOGEE has observed a few OCs to serve as calibrators (see Holtzman et al. 2018). Other OC stars have been observed in the framework of the Open Cluster Chemical Abundances and Mapping (OCCAM) survey (Frinchaboy et al. 2013; Donor et al. 2018) when the clusters were in the field of view of a main survey pointing. Finally, there may also be cluster stars observed by chance among the survey targets. The latter is the main goal of this paper.

We cross-matched the *Gaia* DR2 high-probability OC members with the whole APOGEE DR14 dataset. We excluded those objects flagged in *STARFLAG* as having: many bad pixels ($\geq 40\%$), low signal-to-noise ratio ($S/N \leq 50$ per half-resolution element), or potentially binary stars with significant RV variation between visits ($RV_{\text{scatter}} \geq 5 \text{ km s}^{-1}$). We also rejected those objects that are clearly out of the cluster sequences, which usually have low probabilities, $p \leq 0.6$. Finally, a dozen stars were rejected because they have been reported as non-cluster members on the basis of their RVs in the literature. This step rejects one cluster, Berkeley 44, where the observed star has an astrometric membership of 0.6 but is a field object according to Hayes & Friel (2014). In fact the RV of this star is quite different from the mean value derived for this cluster in the literature.

Cantat-Gaudin et al. (2018) provide discrete astrometric probabilities p for each star to belong to its parent cluster. The value of p takes values between 0.1, least likely, and 1.0, most likely, with a step of 0.1. The derived average RV and chemical abundances can significantly change as a function of the probability threshold used to select the most probable members. Moreover, the total number of OCs for which a mean RV and chemical composition can be computed also depends on the adopted probability cut, as shown in Table 1. Although using a low-probability cut can add stars and clusters to the analysis, it also increases the dispersion of the derived values since some low-probability members are not real members. It is therefore necessary to find an optimal selection threshold. To do so, the strategy developed in Soubiran et al. (2018) has been followed computing the average RV for the 30 clusters with four or more

² We also searched the public *Gaia*-ESO catalogue (DR3, see <https://www.eso.org/qi/>) for unrecognised cluster stars but found only one additional star in one cluster, so we did not proceed further.

Table 1. Number of stars with a membership probability above a given cut, and the corresponding number of OCs with at least one star.

p	Nr Stars	Nr OCs
≥ 0.1	1638	175
≥ 0.2	1559	164
≥ 0.3	1494	152
≥ 0.4	1447	138
≥ 0.5	1406	131
≥ 0.6	1370	129
≥ 0.7	1315	124
≥ 0.8	1222	119
≥ 0.9	1082	108
$=1.0$	852	84

stars with $p = 1$ using different probability cuts. The mean RV values were obtained using

$$RV = \frac{\sum_i RV_i \times g_i}{\sum_i g_i}, \quad (1)$$

where RV_i is the individual RV derived by APOGEE with the weight g_i defined as $g_i = 1/(RV_scatter_i)^2$, where $RV_scatter_i$ is the RV scatter provided by APOGEE.

In Fig. 1 we plot the standard deviation (STDDEV, red), median absolute deviation (MAD; green), and mean (blue) of the difference between the mean RV obtained using different probability cuts, RV_i , and the value obtained using only stars with $p = 1$, $RV_{1.0}$. The mean of the difference does not change significantly for the different cuts, but we see a decrease at $p > 0.5$. The MAD is almost flat for $p \geq 0.4$ and it differs significantly between $p = 0.3$ and $p = 0.4$. The same trend is observed in the standard deviation but in this case the main increase is observed between $p = 0.4$ and $p = 0.5$. As a result of this analysis we limit our analysis to those stars with $p \geq 0.5$. We note that Soubiran et al. (2018) considered members with probabilities $p \geq 0.4$ based on other reference values from the literature.

In total we found 1406 stars with $p \geq 0.5$ belonging to 131 OCs in common between APOGEE DR14 and *Gaia*-DR2 (Cantat-Gaudin et al. 2018). These 131 systems are listed in Table 2. A few examples of colour–magnitude diagrams (CMDs) of these clusters are shown in Fig. 2. The individual stars are listed in Table A.1.

2.2. GALAH

The GALAH survey (De Silva et al. 2015; Martell et al. 2017) is a large observing program using the High Efficiency and Resolution Multi-Element Spectrograph (HERMES, Barden et al. 2010; Sheinis et al. 2015). HERMES provides simultaneous spectra of up to 392 objects with a resolution power of 28 000 in four wavelength bands: 4713–4903 Å (blue arm), 5648–5873 Å (green arm), 6478–6737 Å (red arm), and 7585–7887 Å (infrared arm). The GALAH second Data Release (DR2 Buder et al. 2018) includes about 340 000 stars. Radial velocities and their uncertainties in GALAH are computed by cross-correlating the observed spectra with 15 synthetic AMBRE spectra (de Laverny et al. 2012). The typical RV uncertainty in GALAH DR2 is $\sim 0.1 \text{ km s}^{-1}$ (Zwitter et al. 2018). GALAH chemical analysis is performed in two steps (see, Buder et al. 2018, for details). Briefly, the stellar parameters and abundances of a training set of about 10 500 stars are first found

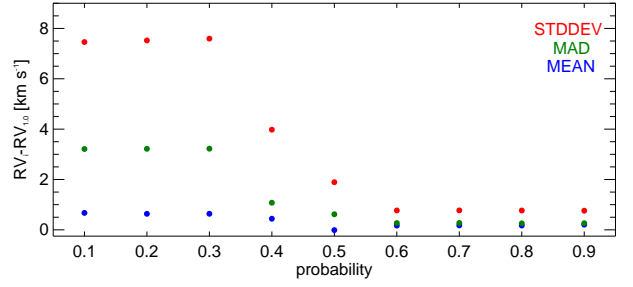


Fig. 1. Run of standard deviation (STDDEV, red), median absolute deviation (MAD, green), and mean (blue) of the difference between the mean RV obtained using different probability cuts and those obtained only for stars with $p = 1$ for the 30 clusters with four or more stars with the highest probability.

by spectral synthesis with the Spectroscopy Made Easy code (SME, Valenti & Piskunov 1996; Piskunov & Valenti 2017). The obtained results are then used to train the *The Cannon* (Ness et al. 2015) data-driven algorithm to find stellar parameters and abundances for the whole GALAH sample.

According to Buder et al. (2018), OCs are not part of the fields already released by GALAH but are observed by several separate programmes with HERMES, that is, with the same instrument. Some OCs were used in Buder et al. (2018) as a test of the GALAH results (see later for further details). Kos et al. (2018b) combined *Gaia* DR2 and GALAH to study five candidate low-density, high-latitude clusters, finding that only one of them, NGC 1901, can be considered a cluster, while the others are only chance projections of stars. Similar results were found by Cantat-Gaudin et al. (2018) for many high-latitude candidate clusters.

While GALAH and the linked private projects are targeting OCs on purpose, there may also be cluster stars observed serendipitously and we looked for them. After cross-matching the Cantat-Gaudin et al. (2018) high-probability members ($p \geq 0.5$) with GALAH DR2 we found 122 stars in 14 OCs. We list in Table A.2 parameters from *Gaia* (G , G_{BP} - G_{RP} , ϖ , μ_{α^*} , μ_{δ}) and GALAH (RV , T_{eff} , $\log g$, $v \sin i$, $[\text{Fe}/\text{H}]$) for the individual stars. Among them, we selected those stars without problems during *The Cannon* analysis, labelled as *flag_cannon=0*, or that need only some extrapolation, *flag_cannon=1* (see Buder et al. 2018, for more details). After applying these constraints we are left with 82 stars in 14 clusters.

Since the majority of the clusters are young, the stars targeted are mostly on the main sequence (MS; there are giants only in NGC 2243 and NGC 2548). Furthermore, they are often of early spectral types and may show high rotational velocities. Their RV determination is therefore less reliable (the same is valid for metallicity; see Sect. 4.2) and we tried to keep only the stars with $v \sin i$ values lower than 20 km s^{-1} . In addition, candidate members according to astrometry show discrepant RVs in some clusters (see Table A.2). To select only the highest-probability cluster members based both on astrometry and RV, we used the average cluster RVs determined by Soubiran et al. (2018) using *Gaia* DR2 data (at least four stars were sampled in all these OCs). This affects only five clusters: ASCC 21, Alessi 24, Alessi-Teutsch 12, NGC 5640, and Turner 5. One discrepant RV star has been discarded in each of them.

After this selection process we ended up with 29 stars in 14 clusters; in half of the cases only one star survived the selections. The properties of these stars are summarised in Table A.3 and Fig. 3 shows the CMD of the 14 OCs and the stars used in our

Table 2. 131 OCs in common between APOGEE DR14 and Cantat-Gaudin et al. (2018).

Cluster	Star type ^a	RV	σ_{RV} (km s ⁻¹)	e_{RV}	Nr	RV_{lit} (km s ⁻¹)	$\sigma_{RV,lit}$ (km s ⁻¹)	Nr_{lit}	RV_{GDR2}^b (km s ⁻¹)	σ_{GDR2}	Nr_{GDR2}	[Fe/H]	$\sigma_{[Fe/H]}$ (dex)	$e_{[Fe/H]}$	Nr	$[Fe/H]_{lit}$ (dex)	$\sigma_{[Fe/H],lit}$ (dex)	Nr_{lit}	Ref.
Alessi 20	MS	-14.89		0.37	1	-11.5	0.01	2	-5.04	3.3	7								1
ASCC 124	MS	-23.35	0.54	0.38	2														
ASCC 16	MS	17.41		0.62	1				23.18	3.4	15								
ASCC 21	MS	16.30	5.66	1.30	19	18.57	2.12	9	18.7	4.45	9	0.01	0.09	0.03	10				2
Basel 11b	RGB	2.68	0.06	0.04	2				3.43	1.46	3	0.014	0.05	0.04	2				
Berkeley 17	RGB	-73.34	0.41	0.13	9	-73.4	0.4	7	-71.95	1.77	7	-0.10	0.04	0.01	9	-0.11	0.03	7	3
Berkeley 19	RGB	17.44	0.0	0.08	1				17.65	0.42	1	-0.22		0.01	1				
Berkeley 29	RGB	25.27	0.53	0.30	3	24.8	1.13	11	50.58	0.94	1								1
Berkeley 31	RGB	57.87	0.65	0.46	2	61.0	3.75	17				-0.305	0.037	0.026	2	-0.31	0.06	2	1,12
Berkeley 33	RGB	77.80	0.56	0.28	4	76.6	0.5	5	78.82	1.12	4	-0.23	0.11	0.05	4				2
Berkeley 43	RGB	29.712		0.136	1				29.15	1.42	9	0.00		0.01	1				
Berkeley 53	RGB	-35.77	0.82	0.29	8	-36.3	0.5	4	-34.9	1.81	7	-0.02	0.03	0.01	6	0.00	0.02	5	3

Notes. ^(a)Type of stars used in the analysis: (RGB) red giant branch, (MS) main sequence, or both. ^(b)From Soubiran et al. (2018). The entire version is available at the CDS.

References. (1) Kharchenko et al. (2013); (2) Dias et al. (2002); (3) Donor et al. (2018); (4) Casamiquela et al. (2016); (5) Carrera et al. (2017); (6) Donati et al. (2015b); (7) Magrini et al. (2017); (8) Schiappacasse-Ulloa et al. (2018); (9) Blanco-Cuaresma et al. (2015); (10) Heiter et al. (2014); (11) Začs et al. (2011); (12) Friel et al. (2010); (13) Monroe & Pilachowski (2010).

analysis are indicated. Table 3 lists the 14 OCs and their mean RVs and metallicities.

3. Radial velocities

3.1. APOGEE

The mean RV for each cluster has been computed using Eq. (1) described above. The internal velocity dispersion is derived as

$$\sigma_{RV} = \sqrt{\frac{n}{n-1} \times \frac{\sum_i g_i \times (RV_i - RV)^2}{\sum_i g_i}}, \quad (2)$$

with an uncertainty of

$$e_{RV} = \frac{\sigma_{RV}}{\sqrt{n}}. \quad (3)$$

For those clusters with only one star sampled we did not compute σ_{RV} and we assumed $e_{RV} = RV_scatter_i$. The obtained values are listed in Table 2. In total we determined a mean RV for 131 clusters. For 78 of them, about 65% of the total, this RV determination is based on less than four stars and the values have to be taken with caution. For the other 53 systems, the RV is determined from four stars or more. In principle these values are more reliable except if they show a large σ_{RV} . Large σ_{RV} values can be due to undetected binaries but also to residual field stars contamination.

For the majority of the OCs, the RV determination is based on either giant or MS stars. In general, the systems whose RVs have been determined from MS stars have larger σ_{RV} values because of the larger RV uncertainties for these stars. There are nine clusters with both kinds of stars sampled: Berkeley 71, Berkeley 85, Berkeley 9, King 7, NGC 1664, NGC 1857, NGC 2682, NGC 6811, and NGC 7782. Except for NGC 1664, at least five stars were observed in each of them. There are no significant differences in the mean RV values if we use only MS stars or giants.

There are 104 clusters in common with the recent work by Soubiran et al. (2018). They derived mean RVs for 861 OCs based on the *Gaia* DR2 catalogue and the RVs obtained with the *Gaia* RVS instrument, using a pre-selection done on our same astrometric membership probabilities (Cantat-Gaudin et al. 2018). The top panel of Fig. 4 shows

the comparison between the RV for the 104 clusters in common. The RV differences, ΔRV , defined as $RV_{Gaia\ DR2} - RV_{APOGEE}$, are shown in the bottom panel of Fig. 4. In general, there is very good agreement between both samples for most of the clusters in spite of the *Gaia* DR2 typical uncertainties being larger than 2.5 km s⁻¹. The median difference between *Gaia* DR2 and our APOGEE sample is 0.4 km s⁻¹ with a median absolute deviation of 3.2 km s⁻¹. However, there are a few cases that show significantly different RVs. All these clusters have only a few sampled stars either in our APOGEE sample or in the *Gaia* DR2 sample. For example, in the case of the system with the largest difference, IC 4996, the values in both samples were obtained for only one candidate member. The RV from the star observed by APOGEE is 78.5 ± 0.3 km s⁻¹, while in *Gaia* DR2, from a different star, the obtained value is -29.1 ± 2.9 km s⁻¹. None of them are similar to the value of -2.5 ± 5.7 km s⁻¹ based on four stars cited in Kharchenko et al. (2013), or to the value of -12 ± 5 km s⁻¹ found from pre-MS stars by Delgado et al. (1999). More data are required in cases such as these.

In addition to the Soubiran et al. (2018) work, we compiled other RV determinations in the literature using the updated version of the DAML and MWSC catalogues as a starting point and adding recent determinations available in the literature. In total we compiled RVs for 75 of the 131 OCs in our sample (see Table 2 where also references are indicated). The comparison between the RV values obtained in this work and the literature is shown in the top panel of Fig. 5, while the bottom panel shows the behaviour of the differences between them. As before, the largest discrepancies are generally observed for those clusters with less than four stars sampled (red points). In fact, the literature determinations for these clusters are also based on four objects or less, with the exception of NGC 457. In Czernik 20 and Trumpler 2 we have seven and five stars, respectively. For Trumpler 2 we found a large σ_{RV} , implying that our RV determination is not very reliable (see below). In the case of Czernik 20, the literature value was obtained from a single star with an uncertainty of 10 km s⁻¹. This value is much larger than the internal dispersion found in our work from seven stars. For this reason we consider our RV determination more reliable.

To our knowledge this is the first RV determination for 16 clusters: ASCC 124, Berkeley 7, Berkeley 98, Czernik 18, Dolidze 3, FSR 0826, FSR 0941, Kronberger 57, L 1641S, NGC 1579, NGC 6469, Ruprecht 148, Stock 4, Teutsch 1,

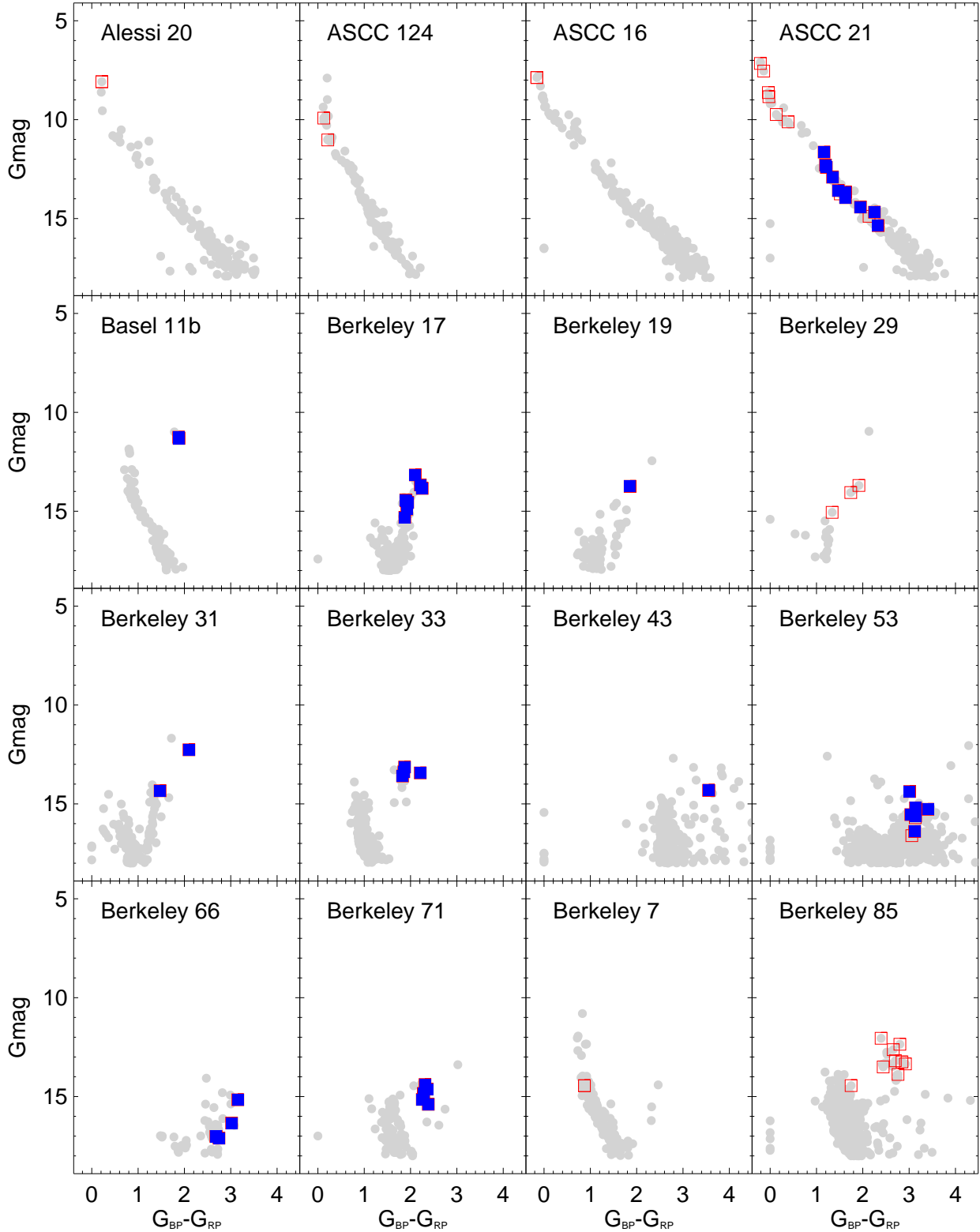


Fig. 2. *Gaia* DR2 CMDs for OCs with stars in common with APOGEE DR14. Grey circles are *Gaia* DR2 stars with a membership probability above 0.5. Open red squares are stars in common with APOGEE DR14 used in the RV determination (see text for details). Filled blue squares are objects used in the [Fe/H] analysis.

Teutsch 12, and Tombaugh 4. In the case of L 1641S our RV determination is based on 43 stars with an internal dispersion of $\sigma_{RV} \sim 2 \text{ km s}^{-1}$. Two clusters, Berkeley 98 and Teutsch 12, have five potential members with a σ_{RV} of 3.3 and 2.3 km s^{-1} , respectively. Due to the number of objects used in these three

systems to derive their mean RV and given their small σ_{RV} , we believe that our determinations are reliable. For the remaining clusters the RV determinations are based on one star only, with the exception of ASCC 124 and Czernik 18, with two and three stars, respectively. As mentioned above, their RVs are less reliable.

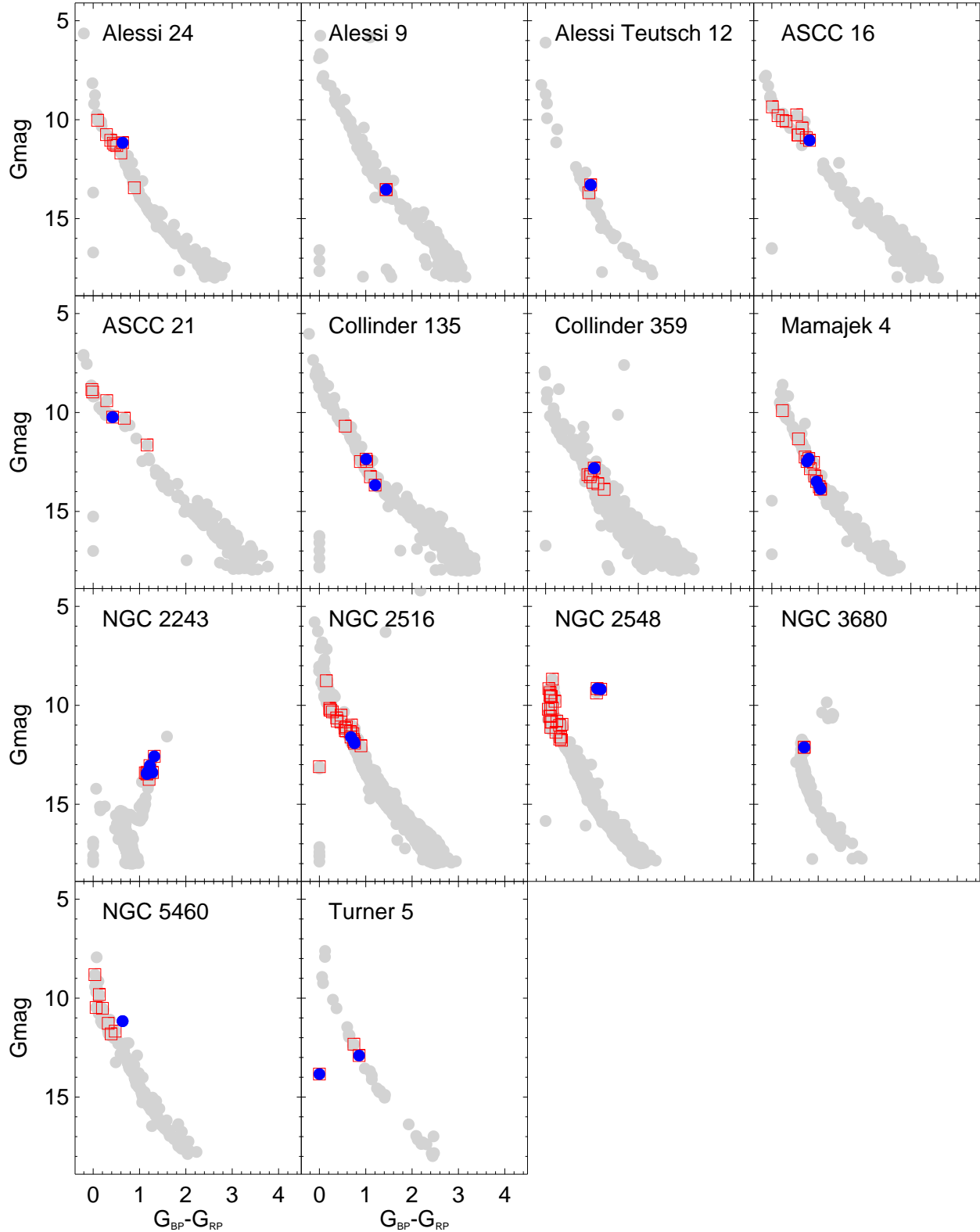


Fig. 3. As in Fig. 2 for the 14 clusters in the GALAH sample. We note that one star in NGC 2516 and one in Turner 5 have no colour information and were arbitrarily plotted at $G_{BP} - G_{RP} = 0$.

Eight systems have σ_{RV} values larger than 6 km s^{-1} . The largest internal dispersion is obtained for NGC 366 with $\sigma_{RV} \sim 21 \text{ km s}^{-1}$. This value was obtained from four stars with $p \geq 0.9$ but with very different individual RVs. In the case of NGC 2183 we found $\sigma_{RV} \sim 13 \text{ km s}^{-1}$. This value is obtained from five

stars with RVs between 7.4 and 43.1 km s^{-1} . However the two stars with the highest priorities, $p = 1$ and 0.8 , have RVs of 28.9 ± 0.2 and $25.4 \pm 0.1 \text{ km s}^{-1}$, respectively. All the stars in NGC 2183 have only one APOGEE visit and therefore the RV determinations are more uncertain. The remaining six clusters

Table 3. Properties of the 14 OCs in common between GALAH DR2 and Cantat-Gaudin et al. (2018).

Cluster	Star type	RV	σ_{RV}	e_{RV} (km s^{-1})	$\langle v \sin i \rangle^{a, \text{star}}$	Nr	RV_{GDR2}^{b}	σ_{GDR2} (km s^{-1})	Nr _{GDR2}	[Fe/H]	$\sigma_{[\text{Fe}/\text{H}]}$ (dex)	$e_{[\text{Fe}/\text{H}]}$	Nr	[Fe/H] _{lit} (dex)	$\sigma_{[\text{Fe}/\text{H}]_{\text{lit}}}$ (dex)	Nr _{lit}	Ref.
Alessi 24	MS	10.44		0.11	11.63	1	12.32	2.24	14	-0.13		0.07	1				
Alessi 9	MS	-5.64		0.11	5.70	1	-6.44	1.14	39	-0.06		0.07	1				
Alessi-Teutsch 12	MS	-11.00		0.12	5.35	1	-5.88	3.54	6	0.40		0.08	1				
ASCC 16	MS	22.01		0.17	38.82 ^c	1	23.18	3.40	15	-0.08 ^d		0.06	1				
ASCC 21	MS	20.05		1.06	19.99 ^c	1	18.70	4.45	9	-0.13 ^d		0.08	1				
Collinder 135	MS	17.08	0.96	0.68	18.31	2	16.03	2.21	51	-0.09	0.03	0.02	2				
Collinder 359	MS	8.30		1.79	57.53 ^c	1	5.28	3.25	12	-0.66 ^d		0.08	1				
Mamajek 4	MS	-28.09	2.19	0.98	6.95	5	-26.32	3.17	34	0.09	0.17	0.08	5				
NGC 2243	RGB	59.32	0.57	0.23	7.36	6	59.63	1.06	4	-0.31	0.05	0.02	6	-0.43	0.04	16	1
NGC 2516	MS	26.01	1.40	0.81	34.10 ^c	3	23.85	2.01	132	-0.26 ^d	0.05	0.03	3	0.06	0.05	13	1
NGC 2548	RGB	8.45	0.40	0.28	5.20	2	8.85	1.08	14	0.16	0.01	0.04	2				
NGC 3680	MS	2.98		1.99	33.54 ^c	1	1.74	1.36	30	-0.26 ^d		0.07	1	-0.01	0.06	10	2
NGC 5460	MS	-5.16	0.31	0.22	23.79 ^c	2	-4.61	2.77	5	-0.32 ^d	0.15	0.11	2				
Turner 5	MS	-2.83	0.09	0.07	11.77	2	-3.49	1.93	6	0.02	0.17	0.12	2				

Notes. ^(a)Mean of the individual values for those clusters with more than one star. ^(b)From Soubiran et al. (2018). ^(c)Values for clusters where $\langle v \sin i \rangle > 20 \text{ km s}^{-1}$ are considered uncertain. ^(d)[Fe/H] uncertain because $\langle v \sin i \rangle > 20 \text{ km s}^{-1}$.

References. (1) Magrini et al. (2017); (2) Netopil et al. (2016)

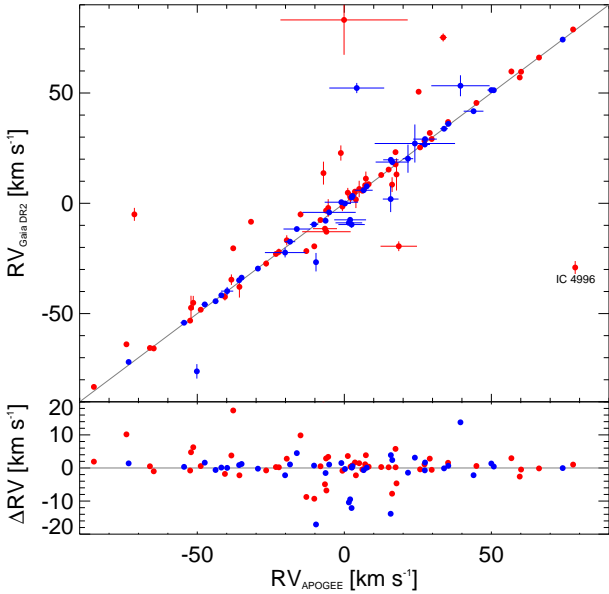


Fig. 4. Comparison between RVs derived from APOGEE DR14 and *Gaia* DR2. Blue points are clusters with four or more stars while red points are systems with less than four stars.

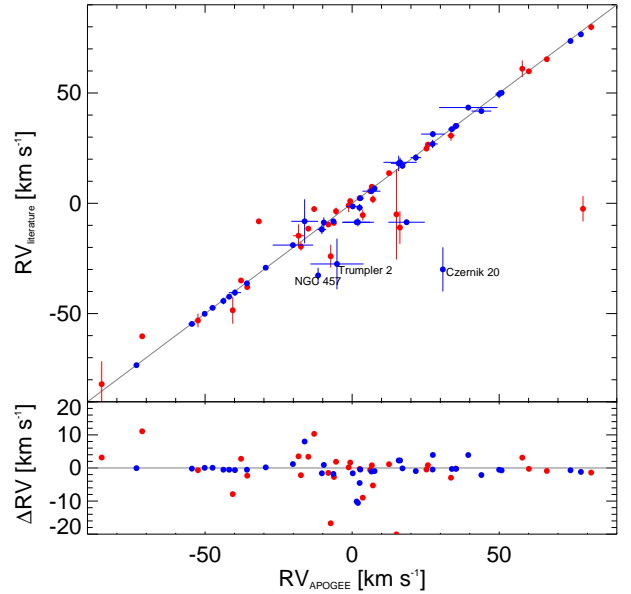


Fig. 5. Comparison between RV derived from APOGEE DR14 and the literature. Blue and red points have the same meaning as in Fig. 4.

(Koposov 36, NGC 2304, NGC 7086, Rosland 6, Trumpler 2, and Trumpler 3) have an σ_{RV} of between 6 and 10 km s^{-1} . The number of potential members sampled by APOGEE in these systems is between four and eight stars. Almost all the stars in these clusters have higher membership probabilities, $p \geq 0.8$. Since all of them are MS stars, their individual RV determination can be affected by the large rotational velocities. Radial velocity determinations are available for three of these in the literature (see Table 2). In spite of the large RV dispersion observed in two of these clusters, NGC 2304 and NGC 7086, we find good agreement with the values listed in the literature (Wu et al. 2009; Kharchenko et al. 2013).

3.2. GALAH

The same procedure followed above for APOGEE was used to derive the mean RV, internal velocity dispersion, and uncertainty

for the 14 OCs in the GALAH sample. The obtained values are listed in Table 3.

Radial velocities for all the clusters in the GALAH sample were recently determined by Soubiran et al. (2018) from *Gaia* DR2. The comparison between the RVs measured by GALAH and those by *Gaia* DR2 for the 14 clusters is shown in Fig. 6. The median difference between *Gaia* DR2 and GALAH is 0.3 km s^{-1} with a median absolute deviation of 1.5 km s^{-1} . The RVs are in reasonable agreement taking into account the fact that the individual RV uncertainties in the *Gaia* DR2 are of 2.5 km s^{-1} on average. The largest differences for some clusters (e.g. Collinder 359 and NGC 2517) are explained by their large average $\langle v \sin i \rangle$ values.

The clusters NGC 2243 and NGC 2516 were also observed by *Gaia*-ESO and their mean RVs are $+60.2$ (rms 1.0) km s^{-1} and $+23.6$ (rms 0.8) km s^{-1} , respectively (Jackson et al. 2016; Magrini et al. 2017). For NGC 2243 we obtained 59.3 km s^{-1}

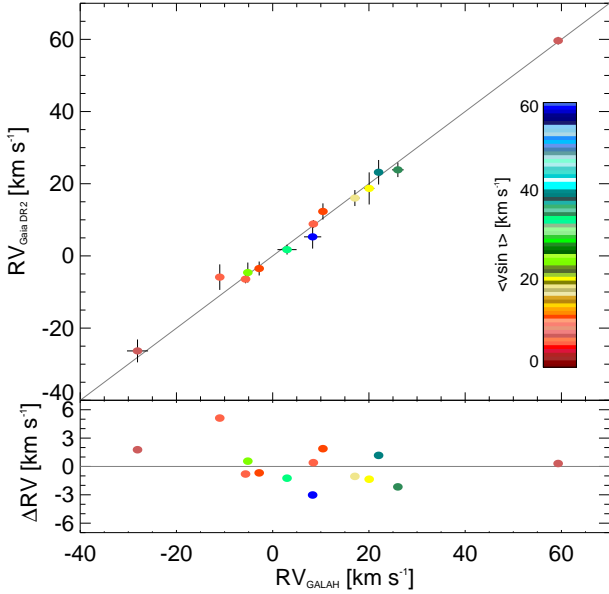


Fig. 6. Comparison between RV derived from GALAH DR2 and *Gaia* DR2, colour-coded according to $\langle v \sin i \rangle$.

with $\sigma_{RV} = 0.6 \text{ km s}^{-1}$ from six giant stars. The values are in good agreement within the uncertainties. In the case of NGC 2516 we obtained 26.0 km s^{-1} with $\sigma_{RV} = 1.4 \text{ km s}^{-1}$ from three MS stars. The difference between GALAH and *Gaia*-ESO mean RVs could be due to the fact that the three stars in the GALAH sample have $v \sin i$ larger than 29 km s^{-1} .

Four of the GALAH clusters are also among the APOGEE systems discussed in the previous section. These clusters are ASCC 16, ASCC 21, Collinder 359, and NGC 2243. In the case of NGC 2243 there is good agreement between the values obtained from both samples in spite of the APOGEE value being based on only one star. For the other three clusters the differences between GALAH and APOGEE are of the order of $\pm 4 \text{ km s}^{-1}$. This is not a large difference taking into account that all the stars sampled in these clusters by GALAH have $v \sin i$ larger than 20 km s^{-1} .

4. Metallicity

4.1. APOGEE

Before deriving average metallicity we excluded the stars for which the ASPCAP pipeline is not able to find a proper solution (or no solution at all) because they are outside of or close to the edges of the synthetic library used in the analysis, such as for example hot stars (see [García Pérez et al. 2016](#); [Holtzman et al. 2018](#), for details). In this case the stars are flagged in *ASPCAPFLAG* as *STAR_BAD* or *NO_ASPCAP_RESULT*, respectively. After rejecting these objects, the sample is reduced to 862 stars belonging to 90 clusters. Most of the rejected stars are fast rotating or low-gravity objects.

Together with the individual iron abundance $[\text{Fe}/\text{H}]$ for each star, APOGEE DR14 provides the scaled-solar general metallicity, $[\text{M}/\text{H}]$. The former is obtained from individual Fe lines whereas the latter is determined as a fundamental atmospheric parameter at the same time as effective temperature, surface gravity, and microturbulent velocity. In this paper we focus on the individual iron abundances. In contrast with the RV case, the average $[\text{Fe}/\text{H}]$ of each cluster was obtained as the unweighted

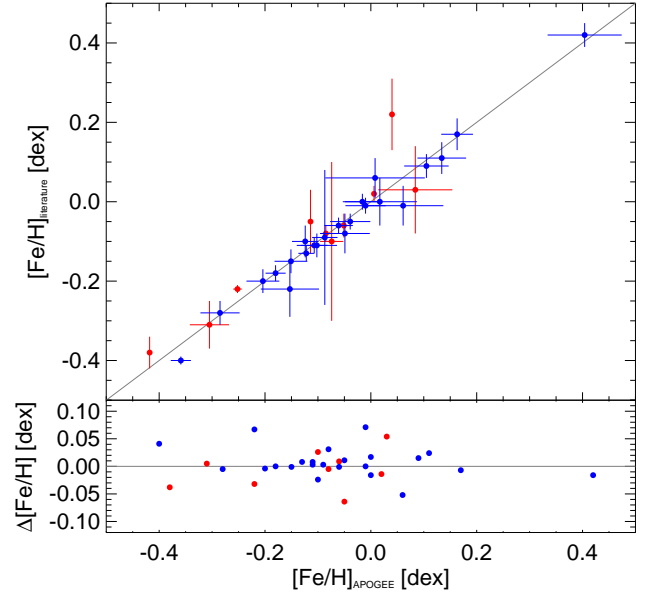


Fig. 7. Comparison between $[\text{Fe}/\text{H}]$ derived from APOGEE DR14 and the literature. Red and blue points are clusters with less or more than four stars, respectively.

mean of the individual iron abundances. We also computed $\sigma_{[\text{Fe}/\text{H}]}$ as the unweighted standard deviation and $e_{[\text{Fe}/\text{H}]}$ as $\frac{\sigma_{[\text{Fe}/\text{H}]}}{\sqrt{n}}$. Other alternatives have been checked because several clusters can be affected by contamination of non-members such as the weighted mean or a Monte Carlo simulation. In the first case we used the individual metallicity uncertainties as weights. For the Monte Carlo simulation, half of the stars in a given cluster were selected randomly and their mean and standard deviation were computed. This procedure was repeated 10^3 times and the cluster mean and σ were obtained as the mean of the individual means and standard deviations. In any case the differences between the obtained values and those derived here are no larger than ± 0.02 dex. Again for those clusters with only one sampled star we did not compute the standard deviation, $\sigma_{[\text{Fe}/\text{H}]}$, and we assume the uncertainty $e_{[\text{Fe}/\text{H}]}$, as the uncertainty for this star, $\sigma_{[\text{Fe}/\text{H}],i}$.

The obtained values are listed in Table 2. For 32 systems our $[\text{Fe}/\text{H}]$ determination is based on four stars or more. With the exception of Berkeley 33, the $\sigma_{[\text{Fe}/\text{H}]}$ is lower than 0.1 dex, which is the typical uncertainty in the APOGEE $[\text{Fe}/\text{H}]$ determination. The $[\text{Fe}/\text{H}]$ determination for the other 58 clusters is based on less than four stars and typically on only one object.

To our knowledge there are previous determinations of iron abundances from high-resolution spectra for a third of the total sample. The comparison between the values derived here and the literature (see Table 2 for references) is shown in Fig. 7. In general, there is very good agreement, with a median difference of 0.00 dex and a median absolute deviation of 0.02 dex. This is not unexpected since several OCs were used as reference to calibrate the whole APOGEE sample assuming values available in the literature (see [Holtzman et al. 2018](#), for details).

For only 9 of the 57 clusters not studied previously, the metallicity determination is based on four or more stars. Two or three stars have been sampled for 16 of these systems. Finally, the metallicity determination for 32 previously unstudied clusters is based on a single star.

4.2. GALAH

In the case of GALAH, the constraints applied initially also ensure that the iron abundance has been determined for all the stars in the sample. The average metallicities for the clusters in the GALAH sample was derived using the same procedure as in the case of APOGEE. The obtained values are listed in Table 3.

Our analysis is based on more than four stars for only two clusters (Mamajek 4 and NGC 2243). The value obtained here for NGC 2243 is in good agreement with the result obtained by Magrini et al. (2017), for example, and other literature sources. This cluster is also among the clusters from APOGEE studied in the previous section. Although the APOGEE analysis is based on a single star, the values are in agreement within the uncertainties.

Due to the early spectral type and high rotational velocity of the members, we judged the metallicity determination for six clusters (ASCC 16, ASCC 21, Collinder 359, NGC 2516, NGC 3680, and NGC 5460) to be unreliable. Moreover, their [Fe/H] values were determined from three stars or less. One of these clusters, ASCC 21, was also analysed from APOGEE data. The values obtained from APOGEE and GALAH samples show a difference of only 0.1 dex, in spite of the large $v \sin i$ and high temperature of the only star in GALAH DR2 for this cluster. Another two of these clusters, NGC 2516 and NGC 3680, have previously been studied by Magrini et al. (2017) and Netopil et al. (2016). In comparison with these works, the [Fe/H] values obtained here are about 0.25 dex lower. Buder et al. (2018) discussed possible shortcomings of the GALAH DR2 catalogue. These latter authors note that the double-step analysis is tailored to single, non-peculiar stars of F, G, and K spectral types and that some systematic trends may be present. In particular, they note difficulties for hot stars (i.e. hotter than late-F spectral type) because they have weaker metal lines, often rotate significantly, and are not present in the training set; all stars hotter than 7000 K are in extrapolation. Furthermore, there is a trend in the derived temperatures, with hotter stars showing lower temperatures than the comparison samples (e.g. the *Gaia* Benchmark stars or stars for which the IRFM was available (see Fig. 14 of Buder et al. 2018)). In turn, this implies a trend towards lower metallicities. This is noticeable, for instance, in the T_{eff} , $\log g$ diagrams for OCs (see Fig. 19 of Buder et al. 2018), with brighter MS stars showing systematically lower abundances. This is also what we found for NGC 2516 and NGC 3680.

In summary, the GALAH DR2 sample provides the first [Fe/H] determination for ten clusters although with different degrees of reliability because of the large rotational velocities of some of the stars analysed.

5. Other elements

5.1. APOGEE

Although APOGEE DR14 provides abundances for 22 chemical elements, not all of them are completely reliable (see Jönsson et al. 2018; Holtzman et al. 2018). For this reason we limit our analysis to the elements that show small systematic differences in comparison with other literature samples according to Jönsson et al. (2018). This includes α -elements (Mg, Si, and Ca) and proton-capture elements (Na and Al) as well as elements of the iron-peak group (Cr, Mn and Ni). For each element, we excluded the stars flagged by ASPCAP with problems in the abundance determination.

We were also able to determine abundances for all the 90 clusters with iron abundances for the majority of elements: Mg, Si, Ca, Mn, and Ni (Table A.4). Aluminum abundances were derived for 89 systems (the missing cluster, IC 1805, has only one star). Several stars were rejected in the determination of chromium content; the abundances of this element were determined for 84 systems. Sodium is the element for which we reject the most stars, with Na abundances obtained for only 65 of the 90 clusters. The abundance of Na is determined in APOGEE from two weak and probably blended lines that are easily measured only in GK giants (see Jönsson et al. 2018, for details). Therefore, Na abundances cannot be determined for many stars in the sample because they are outside this range.

As before, the values obtained here should be used with caution. Only the abundances obtained for at least four stars and with small internal dispersion can be considered reliable. Owing to the large heterogeneity of the abundance determinations available in the literature we have not attempted a comparison.

In Fig. 8 we show trends of the abundance ratios obtained with [Fe/H] and among all other elements. The most discrepant values are due to clusters with less than four stars sampled (grey points). Clusters for which more than four stars were analysed show, in general, a scatter compatible with the typical uncertainties. The exceptions are Na and, to a lesser degree, Cr. The well-known differences of Na abundances between dwarfs and giants due to extra mixing can explain this scatter. There is one cluster, NGC 2168, for which we obtained [Ca/Fe] = -0.17 dex from ten stars. Although this value is lower than the bulk, its dispersion of $\sigma_{[\text{Ca/Fe}]} = 0.21$ dex (probably due to the difficulties in measuring MS stars in APOGEE) makes it still compatible with the majority.

5.2. GALAH

The GALAH DR2 provides abundances for 23 chemical elements including iron (see Buder et al. 2018). For homogeneity with the APOGEE sample, we computed average abundances for the same eight elements as listed in Sect. 5.1. Following the Buder et al. (2018) recommendations we only use those stars that do not have problems in the determination of the abundance of a given element (i.e. $\text{flag_X_FE}=0$). Moreover, we also excluded clusters with $v \sin i > 20 \text{ km s}^{-1}$ because the values obtained for these stars are not reliable. As a result, abundances were determined for only seven clusters and not for all elements. The obtained values are listed in Table A.5.

The GALAH ratios are plotted in Fig. 8 as cyan (less than 4 stars) and blue (more than 4) filled circles. Although the GALAH sample is small, we see that there are no significant differences between APOGEE and GALAH samples for any of the elements studied. Only the metal-poor cluster NGC 2243 seems to have a large [Ni/Fe] ratio, +0.22 dex ($\sigma_{[\text{Ni/Fe}]} = 0.14$ dex) obtained from five stars, in comparison with other APOGEE clusters of the same [Fe/H]. This cluster is the only one in common with the APOGEE sample with reliable abundances in GALAH. For a direct comparison, in the case of APOGEE we obtained [Ni/Fe] = 0.01 dex from a single star with $e_{[\text{Ni/Fe}]} = 0.02$ dex. Also for Si we found a difference larger than the uncertainties: [Si/Fe] = 0.09 and -0.04 dex from APOGEE and GALAH, respectively. Again the APOGEE value was derived from a single star with $e_{[\text{Si/Fe}]} = 0.03$ dex while the GALAH one was determined from four stars with $\sigma_{[\text{Ni/Fe}]} = 0.04$ dex. For the other elements studied, the ratios obtained from APOGEE and GALAH samples are in agreement within the uncertainties.

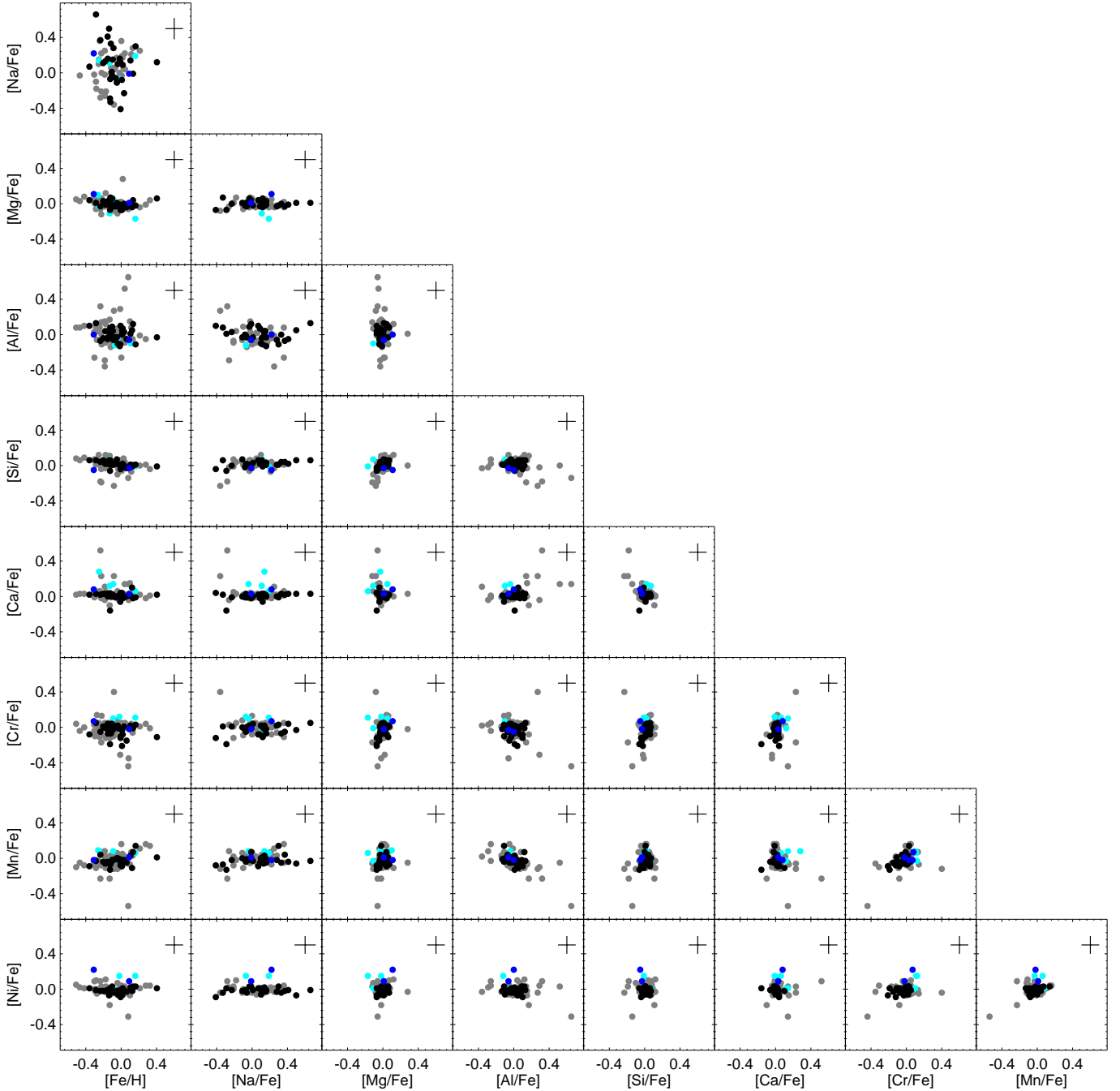


Fig. 8. Abundance ratios for APOGEE and GALAH clusters. Grey and black circles are APOGEE clusters with less and more than four stars in the determination of $[\text{Fe}/\text{H}]$, respectively. Cyan and blue circles are GALAH clusters with less and more than four stars in the determination of $[\text{Fe}/\text{H}]$, respectively. Typical error bars are plotted in the top-right corners.

6. Galactic trends

As mentioned in Sect. 1, information about the chemical composition of OCs is necessary to address a variety of astrophysical topics. A clear example of the applicability of the sample obtained in this work is the study of the chemical gradients in the Galactic disc. Generally, the chemical gradients in the Galactic disc are studied using iron (e.g. Netopil et al. 2016), which is produced in approximately equal measure by core collapse and type Ia supernovae. Additionally, we present here the behaviour of magnesium as best representative of the α -elements. Not only is the production of magnesium dominated by core-collapse supernovae, but also the Mg abundances

derived by APOGEE and GALAH show the best agreement with external measurements in comparison with other elements of this group (Jönsson et al. 2018; Buder et al. 2018). Given the much larger number of clusters involved, the APOGEE data dominate the following discussion. The run of $[\text{Fe}/\text{H}]$ as a function of Galactocentric distance, R_{gc} , is plotted in the bottom panel of Fig. 9, while the top panel shows the behaviour of $[\text{Mg}/\text{Fe}]$ with R_{gc} . Galactocentric distances were computed by Cantat-Gaudin et al. (2018) from *Gaia*-DR2 parallaxes; we refer the reader to that paper for details of the distance determination.

The clusters with four or more stars, that is those for which more trustworthy measurements are available (blue symbols), cover a range in R_{gc} between ~ 6.5 and ~ 13 kpc. Grey

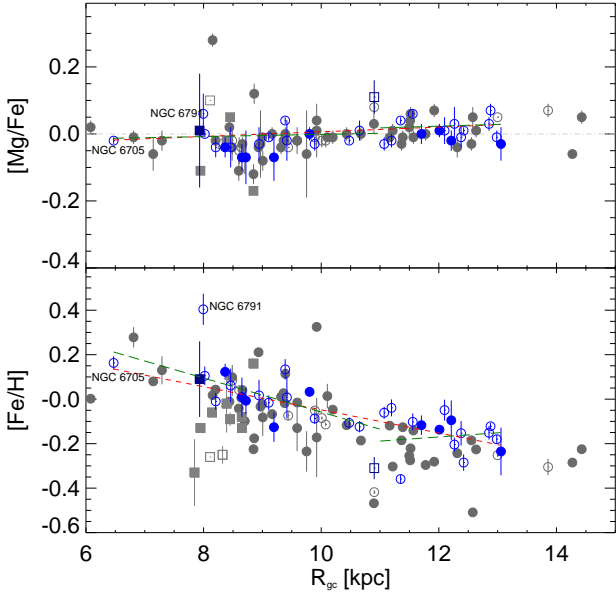


Fig. 9. Gradient in $[Mg/Fe]$ (*top panel*) and $[Fe/H]$ (*bottom panel*) as a function of R_{gc} for APOGEE (circles) and GALAH (triangles) clusters. Grey symbols are clusters with less than four stars. Blue symbols are clusters with four or more stars sampled. Filled symbols are the clusters for which this is the first metallicity determination from high-resolution spectroscopy. Green and orange lines show different linear fits (see text for details). The positions of NGC 6705 and NGC 6791 are marked.

symbols are clusters with less-reliable measurements. The slope of the gradient in this R_{gc} range is debated and we find values between $\frac{d[Fe/H]}{dR_{gc}} \sim -0.035 \text{ dex kpc}^{-1}$ (Cunha et al. 2016) and $-0.1 \text{ dex kpc}^{-1}$ (Jacobson et al. 2016) in the literature. Using all the clusters in the APOGEE and GALAH samples with at least four stars we found $\frac{d[Fe/H]}{dR_{gc}} = -0.052 \pm 0.003 \text{ dex kpc}^{-1}$ (red dashed line). The slope of the gradients may depend on the presence of the innermost cluster in the sample, NGC 6705, and the most metal-rich one, NGC 6791. Both are peculiar clusters. NGC 6705 is a young metal-rich system (see e.g. Cantat-Gaudin et al. 2014) with an unexpectedly high abundance in α -elements (Casamiquela et al. 2018; Magrini et al. 2017). On the contrary, NGC 6791 is an intriguing, old, very metal-rich, and massive system located almost 1 kpc above the Galactic plane. It has been suggested that NGC 6791 has likely migrated to its current location from its birth position (Linden et al. 2017) or even has an extragalactic origin (Carraro et al. 2006), although both claims are disputed. If we exclude these two clusters from the analysis, the $[Fe/H]$ gradient flattens to $-0.047 \pm 0.004 \text{ dex kpc}^{-1}$. This does not imply that the former value is preferred. It only shows how the gradient changes as a function of the outliers.

If we separate the clusters in two groups inside and outside $R_{gc} = 11 \text{ kpc}$ we find $\frac{d[Fe/H]}{dR_{gc}} = -0.077 \pm 0.007 \text{ dex kpc}^{-1}$ in the inner region and $\frac{d[Fe/H]}{dR_{gc}} = 0.018 \pm 0.009 \text{ dex kpc}^{-1}$ for the outer region. A similar result has previously been reported (e.g. Carrera & Pancino 2011; Andreuzzi et al. 2011; Frinchaboy et al. 2013; Cantat-Gaudin et al. 2016, among many). If we exclude the two metal-poor cluster at $R_{gc} \sim 11 \text{ kpc}$ (NGC 2243 and Trumpler 5) the slope increases until $\frac{d[Fe/H]}{dR_{gc}} = -0.04 \pm 0.01 \text{ dex kpc}^{-1}$. Therefore, the behaviour in the outermost region is highly dependent on these clusters. All these results

are in good agreement with Donor et al. (2018) who also used chemical abundances obtained from APOGEE DR14 with a different cluster membership selection. Furthermore, the observed gradient may change as a function of the age of the clusters used in the analysis (e.g. Friel et al. 2002; Andreuzzi et al. 2011; Carrera & Pancino 2011; Jacobson et al. 2016). However, age is yet unknown for a large fraction of our clusters and we postpone a detailed analysis of the evolution of the gradient with the age of the clusters to a forthcoming paper.

The run of α -element abundances as a function of Galactocentric radius is still an open discussion (e.g. Donati et al. 2015a; Cantat-Gaudin et al. 2016). Donor et al. (2018) report a mild positive gradient for magnesium and other α -elements such as oxygen or silicon. In contrast, Yong et al. (2012) and Friel et al. (2014) found no dependence with R_{gc} . A similar result was found by Cantat-Gaudin et al. (2016) and also by Magrini et al. (2017) using OCs and field stars homogeneously analysed by the *Gaia*-ESO survey. The top panel of Fig. 9 does not show a clear trend. The slope of the linear fit (red dashed line) to the whole range of R_{gc} is $\frac{d[Mg/Fe]}{dR_{gc}} = 0.003 \pm 0.002 \text{ dex kpc}^{-1}$. The clusters within $R_{gc} \sim 10 \text{ kpc}$ have, in general, a $[Mg/Fe]$ below the solar one. This includes the innermost cluster, NGC 6705, for which Casamiquela et al. (2018) report a higher value of $[Mg/Fe] = +0.14 \pm 0.07 \text{ dex}$, in agreement with the *Gaia*-ESO result of $+0.10 \pm 0.07$ (Magrini et al. 2017). There is a group of clusters at $\sim 8 \text{ kpc}$ which $[Mg/Fe]$ are compatible with the solar one within uncertainties. At $R_{gc} \sim 8.5 \text{ kpc}$, the $[Mg/Fe]$ is clearly lower than the solar; from there the $[Mg/Fe]$ ratio increases until $\sim 10 \text{ kpc}$, whereafter it flattens out. This behaviour has been reported previously in the literature (e.g. Cantat-Gaudin et al. 2016; Magrini et al. 2017) and has been predicted by Galactic chemical evolution models (e.g. Minchev et al. 2014; Kubryk et al. 2015a,b; Grisoni et al. 2018).

The existence of a vertical gradient is also controversial. Several authors do not find any trend of $[Fe/H]$ with the distance to the Galactic plane, Z (e.g. Jacobson et al. 2011; Carrera & Pancino 2011). Instead, other studies reported the existence of a vertical gradient with a slope between -0.34 and $-0.25 \text{ dex kpc}^{-1}$ (e.g. Piatti et al. 1995; Carraro et al. 1998). In Fig. 10 we plot $[Fe/H]$ and $[Mg/Fe]$ as a function of Z (bottom and upper panel, respectively). In both cases there are no signs of the existence of vertical gradients, in agreement with most previous studies. We also confirm that clusters located at larger Galactocentric distances cover a larger range of Z . One exception is NGC 6791 located at $R_{gc} \sim 8 \text{ kpc}$ and with a height above the plane of $Z \sim 900 \text{ pc}$. We have already mentioned that this is a peculiar system that is not well understood.

7. Summary

Using *Gaia* DR2, Cantat-Gaudin et al. (2018) determined astrometric membership probabilities for stars belonging to 1229 OCs. We cross-matched this catalogue with the latest data releases of two of the largest Galactic high-resolution spectroscopic surveys, APOGEE and GALAH, with the goal of finding high-probability OC members.

- In the case of APOGEE we detected stars belonging to 131 clusters for which we determined average RVs. For 46 systems, our determination is based on four or more stars. To our knowledge this is the first RV determination for 16 systems. For the other clusters there is good agreement between the obtained values and those available in the literature. $[Fe/H]$ was obtained for 90 OCs, almost two thirds of them

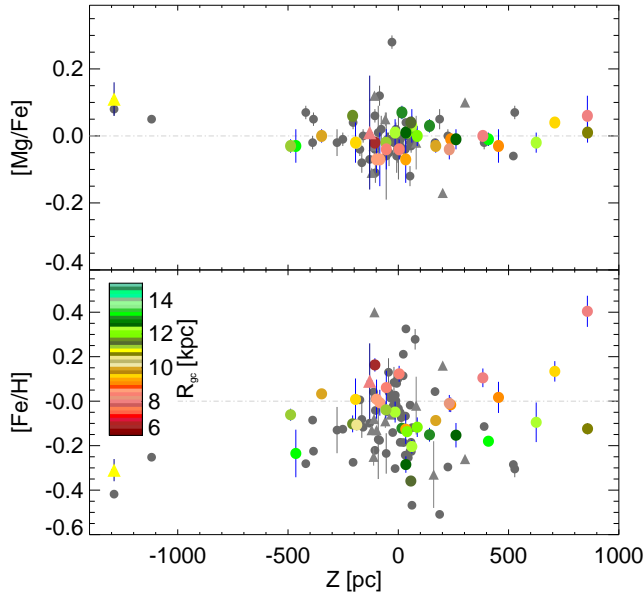


Fig. 10. Run of $[Mg/Fe]$ (top panel) and $[Fe/H]$ (bottom panel) as a function of the distance to the Galactic plane Z . Symbols are as in Fig. 9.

without previous determinations in the literature. Finally, for the same 90 clusters we also determined abundances for six elements: Na, Mg, Al, Si, Ca, Cr, Mn, and Ni.

- In the case of GALAH we found stars belonging to 14 clusters for which we determined both RVs and iron abundances. With the exception of two clusters, NGC 2243 and NGC 2548, the GALAH sample is composed of MS stars, in some cases with significant $v \sin i$ values. These 14 clusters have previous RV determinations from *Gaia* DR2. Excluding the two clusters in common with the APOGEE sample, nine of these systems do not have previous determinations in the literature from high-resolution spectroscopy. For seven clusters we determined abundances for the same chemical elements as those studied in the APOGEE catalogue.

In summary, to our knowledge this is the first RV determination from high-resolution spectra for 16 OCs. Similarly, we provide for the first time iron abundances for 39 OCs, 30 from APOGEE and 9 from GALAH, respectively.

The obtained catalogue of chemical abundances was used to investigate the existence of radial and vertical trends using the distances computed from *Gaia* DR2. Our findings are in agreement with previous investigations where the radial $[Fe/H]$ gradient appears to flatten in the outer region. We do not find any evidence, at least above the 1σ level, of the existence of a vertical metallicity gradient.

Acknowledgements. This work has made use of data from the European Space Agency (ESA) mission *Gaia* (<https://www.cosmos.esa.int/gaia>), processed by the *Gaia* Data Processing and Analysis Consortium (DPAC, <https://www.cosmos.esa.int/web/gaia/dpac/consortium>). Funding for the DPAC has been provided by national institutions, in particular the institutions participating in the *Gaia* Multilateral Agreement. This work has made use of APOGEE data. Funding for the Sloan Digital Sky Survey IV has been provided by the Alfred P. Sloan Foundation, the U.S. Department of Energy Office of Science, and the Participating Institutions. SDSS-IV acknowledges support and resources from the Center for High-Performance Computing at the University of Utah. The SDSS web site is www.sdss.org. SDSS-IV is managed by the Astrophysical Research Consortium for the Participating Institutions of the SDSS Collaboration including the Brazilian Participation Group, the Carnegie Institution for Science, Carnegie Mellon University, the Chilean Participation Group, the French Participation Group, Harvard-Smithsonian Center for

Astrophysics, Instituto de Astrofísica de Canarias, The Johns Hopkins University, Kavli Institute for the Physics and Mathematics of the Universe (IPMU)/University of Tokyo, the Korean Participation Group, Lawrence Berkeley National Laboratory, Leibniz Institut für Astrophysik Potsdam (AIP), Max-Planck-Institut für Astronomie (MPIA Heidelberg), Max-Planck-Institut für Astrophysik (MPA Garching), Max-Planck-Institut für Extraterrestrische Physik (MPE), National Astronomical Observatories of China, New Mexico State University, New York University, University of Notre Dame, Observatório Nacional / MCTI, The Ohio State University, Pennsylvania State University, Shanghai Astronomical Observatory, United Kingdom Participation Group, Universidad Nacional Autónoma de México, University of Arizona, University of Colorado Boulder, University of Oxford, University of Portsmouth, University of Utah, University of Virginia, University of Washington, University of Wisconsin, Vanderbilt University, and Yale University. This work has made use of GALAH data, based on data acquired through the Australian Astronomical Observatory, under programmes: A/2013B/13 (The GALAH pilot survey); A/2014A/25, A/2015A/19, and A2017A/18 (The GALAH survey). We acknowledge the traditional owners of the land on which the AAT stands, the Gamilaraay people, and pay our respects to elders past and present. This research has made use of VizieR and SIMBAD, operated at CDS, Strasbourg, France, NASA's Astrophysical Data System, and TOPCAT (<http://www.starlink.ac.uk/topcat/>, Taylor et al. 2005). This research made use of the cross-match service provided by CDS, Strasbourg. This work was partly supported by the MINECO (Spanish Ministry of Economy) through grant ESP2016-80079-C2-1-R (MINECO/FEDER, UE) and MDM-2014-0369 of ICCUB (Unidad de Excelencia “María de Maeztu”). A.B. acknowledges funding from PREMIALE 2015 MITiC.

References

- Abolfathi, B., Aguado, D. S., Aguilar, G., et al. 2018, *ApJS*, 235, 42
 Anders, F., Chiappini, C., Minchev, I., et al. 2017, *A&A*, 600, A70
 Andruzzi, G., Bragaglia, A., Tosi, M., & Marconi, G. 2011, *MNRAS*, 412, 1265
 Bailor-Jones, C. A. L., Andrae, R., Arcay, B., et al. 2013, *A&A*, 559, A74
 Barden, S. C., Jones, D. J., Barnes, S. I., et al. 2010, in *Ground-based and Airborne Instrumentation for Astronomy III*, Proc. SPIE, 7735, 773509
 Blanco-Cuaresma, S., Soubiran, C., Heiter, U., et al. 2015, *A&A*, 577, A47
 Blanton, M. R., Bershady, M. A., Abolfathi, B., et al. 2017, *AJ*, 154, 28
 Bovy, J. 2016, *ApJ*, 817, 49
 Buder, S., Asplund, M., Duong, L., et al. 2018, *MNRAS*, 478, 4513
 Cantat-Gaudin, T., Vallenari, A., Zaggia, S., et al. 2014, *A&A*, 569, A17
 Cantat-Gaudin, T., Donati, P., Vallenari, A., et al. 2016, *A&A*, 588, A120
 Cantat-Gaudin, T., Jordi, C., Vallenari, A., et al. 2018, *A&A*, 618, A93
 Carraro, G., Ng, Y. K., & Portinari, L. 1998, *MNRAS*, 296, 1045
 Carraro, G., Villanova, S., Demarque, P., et al. 2006, *ApJ*, 643, 1151
 Carrera, R., & Pancino, E. 2011, *A&A*, 535, A30
 Carrera, R., Rodríguez Espinosa, L., Casamiquela, L., et al. 2017, *MNRAS*, 470, 4285
 Casamiquela, L., Carrera, R., Jordi, C., et al. 2016, *MNRAS*, 458, 3150
 Casamiquela, L., Carrera, R., Blanco-Cuaresma, S., et al. 2017, *MNRAS*, 470, 4363
 Casamiquela, L., Carrera, R., Balaguer-Núñez, L., et al. 2018, *A&A*, 610, A66
 Cunha, K., Frinchaboy, P. M., Souto, D., et al. 2016, *Astron. Nachr.*, 337, 922
 de Laverny, P., Recio-Blanco, A., Worley, C. C., & Plez, B. 2012, *A&A*, 544, A126
 Delgado, A. J., Miranda, L. F., & Alfaro, E. J. 1999, *AJ*, 118, 1759
 De Silva, G. M., Freeman, K. C., Asplund, M., et al. 2007, *AJ*, 133, 1161
 De Silva, G. M., Freeman, K. C., Bland-Hawthorn, J., et al. 2015, *MNRAS*, 449, 2604
 Dias, W. S., Alessi, B. S., Moitinho, A., & Lépine, J. R. D. 2002, *A&A*, 389, 871
 Donati, P., Bragaglia, A., Carretta, E., et al. 2015a, *MNRAS*, 453, 4185
 Donati, P., Cocozza, G., Bragaglia, A., et al. 2015b, *MNRAS*, 446, 1411
 Donor, J., Frinchaboy, P. M., Cunha, K., et al. 2018, *AJ*, 156, 142
 Eisenstein, D. J., Weinberg, D. H., Agol, E., et al. 2011, *AJ*, 142, 72
 Evans, D. W., Riello, M., De Angeli, F., et al. 2018, *A&A*, 616, A4
 Friel, E. D., Janes, K. A., Tavares, M., et al. 2002, *AJ*, 124, 2693
 Friel, E. D., Jacobson, H. R., & Pilachowski, C. A. 2010, *AJ*, 139, 1942
 Friel, E. D., Donati, P., Bragaglia, A., et al. 2014, *A&A*, 563, A117
 Frinchaboy, P. M., Thompson, B., Jackson, K. M., et al. 2013, *ApJ*, 777, L1
 Gaia Collaboration (Prusti, T., et al.) 2016, *A&A*, 595, A1
 Gaia Collaboration (Brown, A. G. A., et al.) 2018, *A&A*, 616, A1
 García Pérez, A. E., Allende Prieto, C., Holtzman, J. A., et al. 2016, *AJ*, 151, 144
 Gilmore, G., Randich, S., Asplund, M., et al. 2012, *The Messenger*, 147, 25
 Grisoni, V., Spitoni, E., & Matteucci, F. 2018, *MNRAS*, 481, 2570
 Hayes, C. R., & Friel, E. D. 2014, *AJ*, 147, 69
 Heiter, U., Soubiran, C., Netopil, M., & Paunzen, E. 2014, *A&A*, 561, A93
 Holtzman, J. A., Hesselquist, S., Shetrone, M., et al. 2018, *AJ*, 156, 125

- Jackson, R. J., Jeffries, R. D., Randich, S., et al. 2016, *A&A*, 586, A52
- Jacobson, H. R., Pilachowski, C. A., & Friel, E. D. 2011, *AJ*, 142, 59
- Jacobson, H. R., Friel, E. D., Jílková, L., et al. 2016, *A&A*, 591, A37
- Jönsson, H., Allende Prieto, C., Holtzman, J. A., et al. 2018, *AJ*, 156, 126
- Katz, D., Sartoretti, P., Cropper, M., et al. 2019, *A&A*, 622, A205
- Kharchenko, N. V., Piskunov, A. E., Schilbach, E., Röser, S., & Scholz, R.-D. 2013, *A&A*, 558, A53
- Kos, J., de Silva, G., Buder, S., et al. 2018a, *MNRAS*, 480, 5242
- Kos, J., Bland-Hawthorn, J., Freeman, K., et al. 2018b, *MNRAS*, 473, 4612
- Krone-Martins, A., & Moitinho, A. 2014, *A&A*, 561, A57
- Kubryk, M., Prantzos, N., & Athanassoula, E. 2015a, *A&A*, 580, A126
- Kubryk, M., Prantzos, N., & Athanassoula, E. 2015b, *A&A*, 580, A127
- Lindgren, L., Hernández, J., Bombrun, A., et al. 2018, *A&A*, 616, A2
- Linden, S. T., Pryal, M., Hayes, C. R., et al. 2017, *ApJ*, 842, 49
- Liu, F., Yong, D., Asplund, M., Ramírez, I., & Meléndez, J. 2016, *MNRAS*, 457, 3934
- Magrini, L., Randich, S., Kordopatis, G., et al. 2017, *A&A*, 603, A2
- Majewski, S. R., Schiavon, R. P., Frinchaboy, P. M., et al. 2017, *AJ*, 154, 94
- Martell, S. L., Sharma, S., Buder, S., et al. 2017, *MNRAS*, 465, 3203
- Minchev, I., Chiappini, C., & Martig, M. 2014, *A&A*, 572, A92
- Monroe, T. R., & Pilachowski, C. A. 2010, *AJ*, 140, 2109
- Ness, M., Hogg, D. W., Rix, H.-W., Ho, A. Y. Q., & Zasowski, G. 2015, *ApJ*, 808, 16
- Netopil, M., Paunzen, E., Heiter, U., & Soubiran, C. 2016, *A&A*, 585, A150
- Nidever, D. L., Holtzman, J. A., Allende Prieto, C., et al. 2015, *AJ*, 150, 173
- Piatti, A. E., Claria, J. J., & Abadi, M. G. 1995, *AJ*, 110, 2813
- Piskunov, N., & Valenti, J. A. 2017, *A&A*, 597, A16
- Randich, S., Gilmore, G., & Gaia-ESO Consortium 2013, *The Messenger*, 154, 47
- Randich, S., Tognelli, E., Jackson, R., et al. 2018, *A&A*, 612, A99
- Reddy, A. B. S., Lambert, D. L., & Giridhar, S. 2016, *MNRAS*, 463, 4366
- Roškar, R., Debattista, V. P., Quinn, T. R., Stinson, G. S., & Wadsley, J. 2008, *ApJ*, 684, L79
- Sartoretti, P., Katz, D., Cropper, M., et al. 2018, *A&A*, 616, A6
- Schiappacasse-Ulloa, J., Tang, B., Fernández-Trincado, J. G., et al. 2018, *AJ*, 156, 94
- Sheinis, A., Anguiano, B., Asplund, M., et al. 2015, *J. Astron. Telescopes, Instrum. Syst.*, 1, 035002
- Soubiran, C., Cantat-Gaudin, T., Romero-Gómez, M., et al. 2018, *A&A*, 619, A155
- Taylor, M. B. 2005, in *Astronomical Data Analysis Software and Systems XIV*, eds. P. Shopbell, M. Britton, & R. Ebert, *ASP Conf. Ser.*, 347, 29
- Valenti, J. A., & Piskunov, N. 1996, *A&AS*, 118, 595
- Wu, Z.-Y., Zhou, X., Ma, J., & Du, C.-H. 2009, *MNRAS*, 399, 2146
- Yong, D., Carney, B. W., & Friel, E. D. 2012, *AJ*, 144, 95
- Začs, L., Alksnis, O., Barzdis, A., et al. 2011, *MNRAS*, 417, 649
- Zwitter, T., Kos, J., Chiavassa, A., et al. 2018, *MNRAS*, 481, 645

Appendix A: Additional material

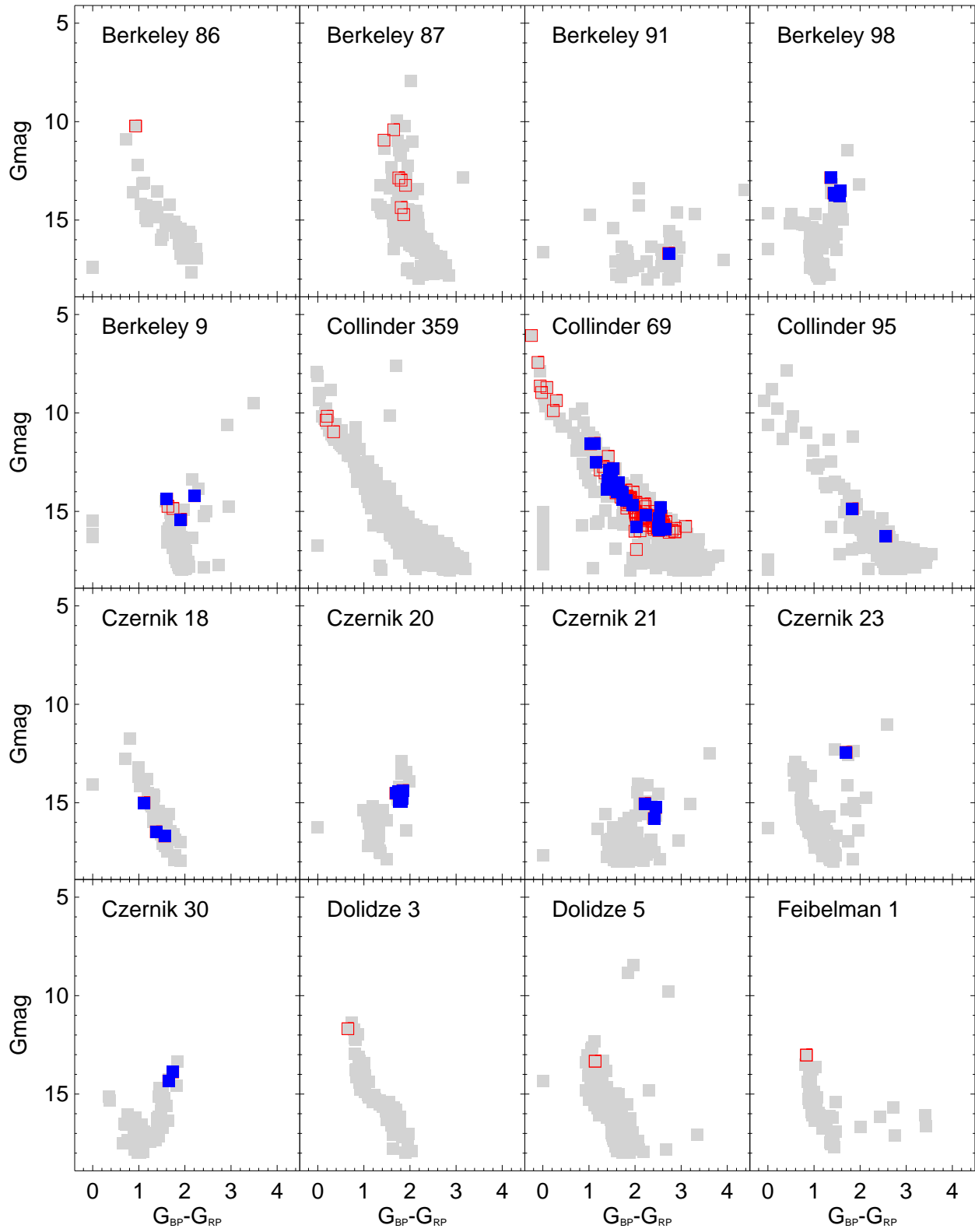


Fig. A.1. Continuation of Fig. 2.

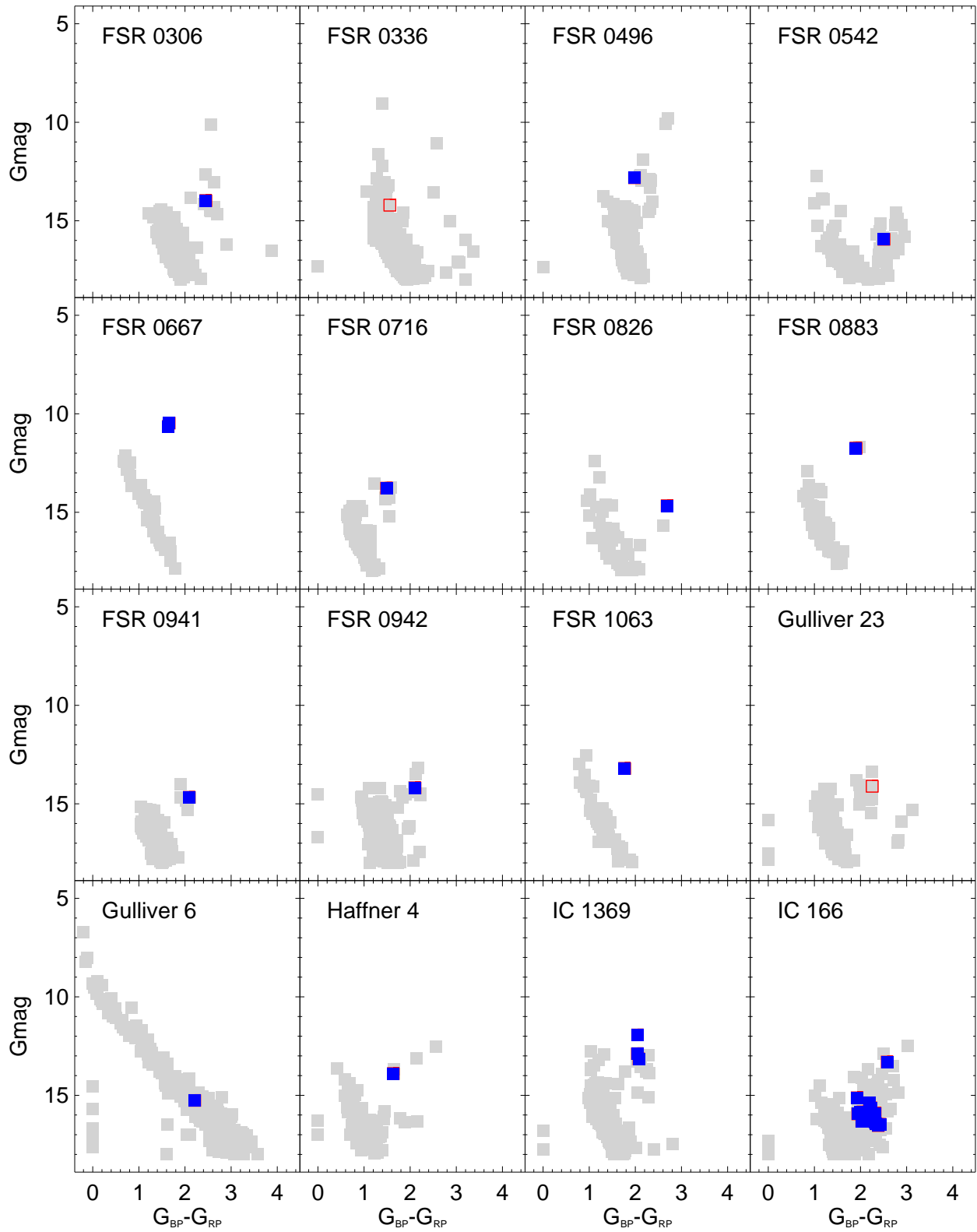


Fig. A.1. continued.

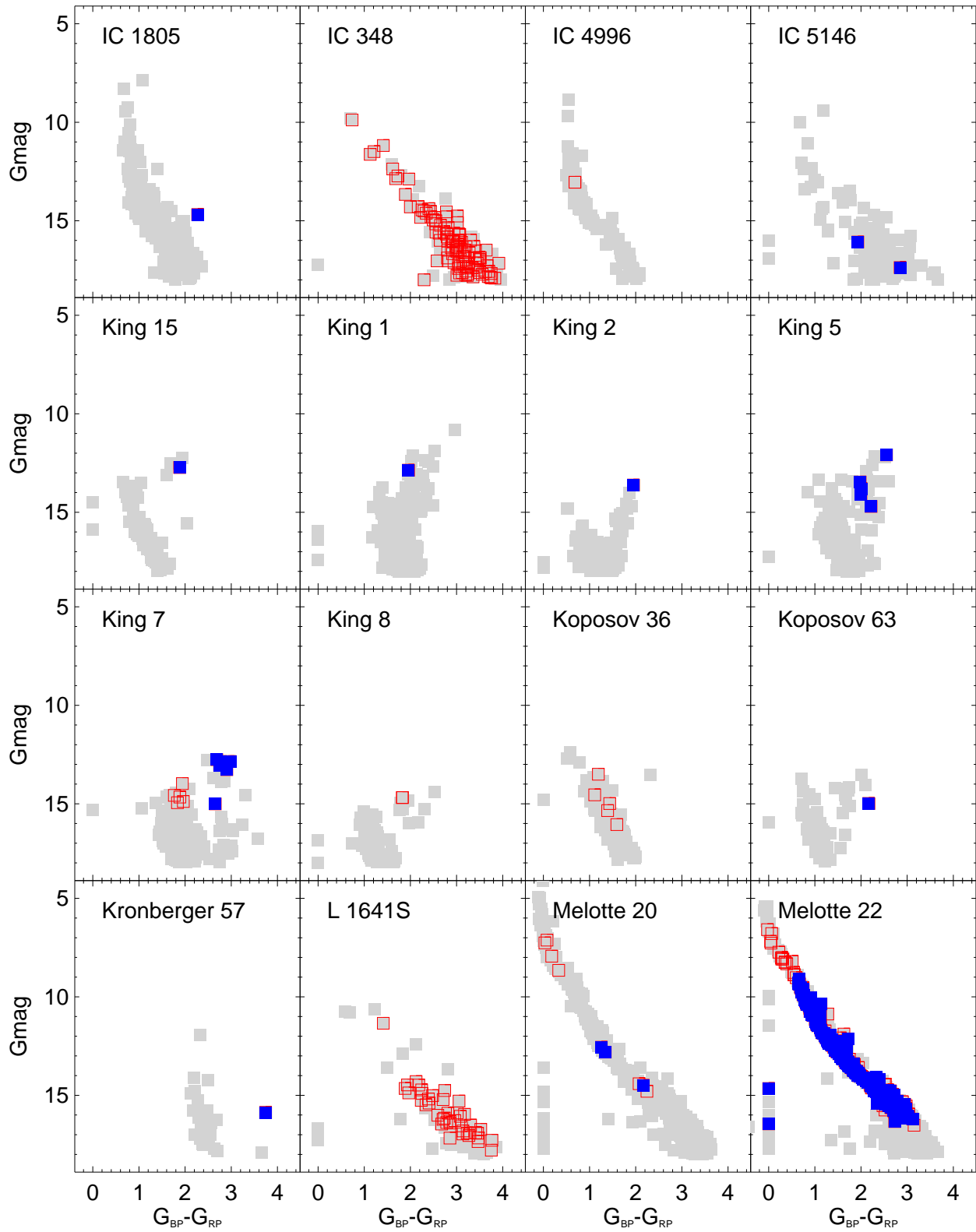


Fig. A.1. continued.

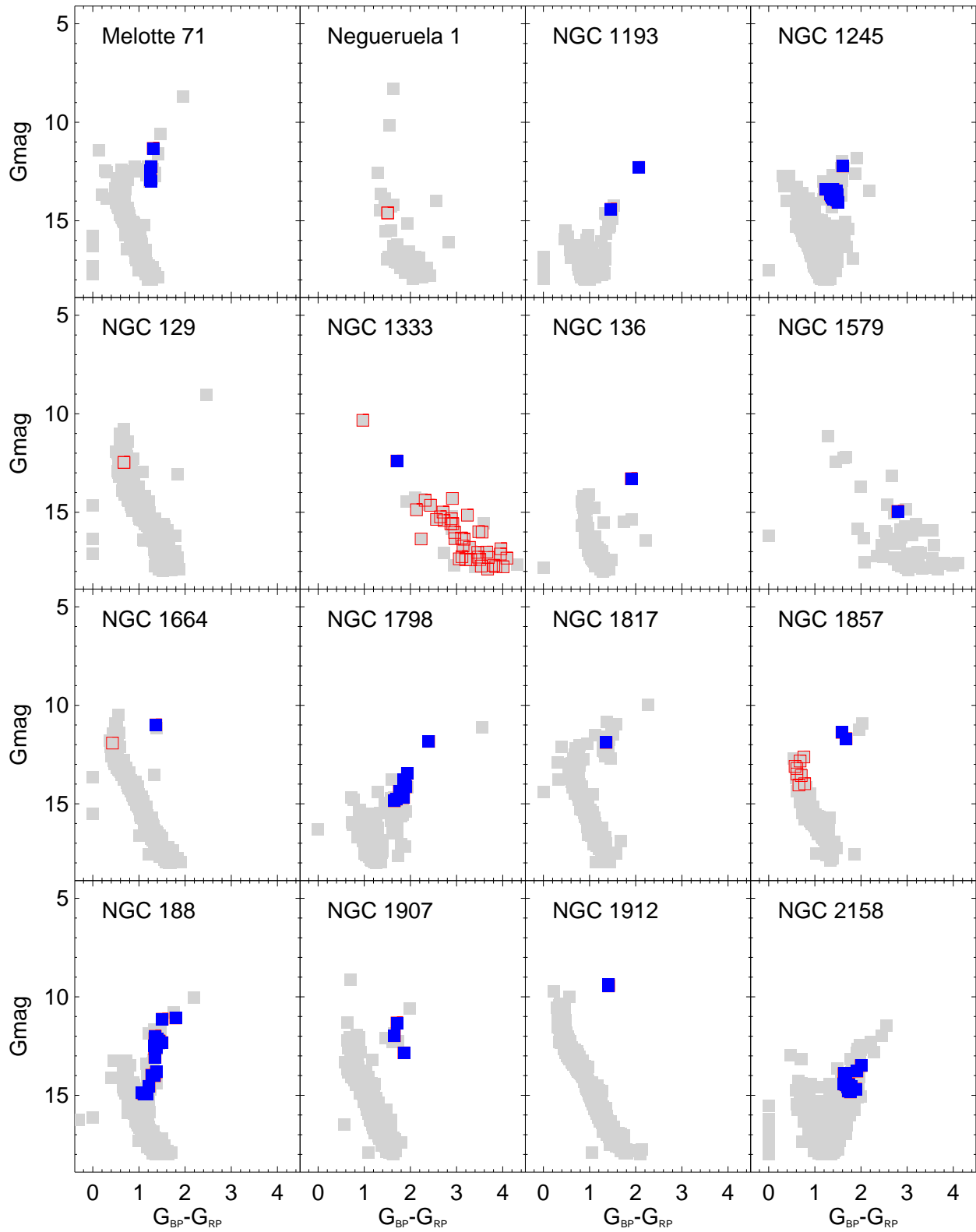


Fig. A.1. continued.

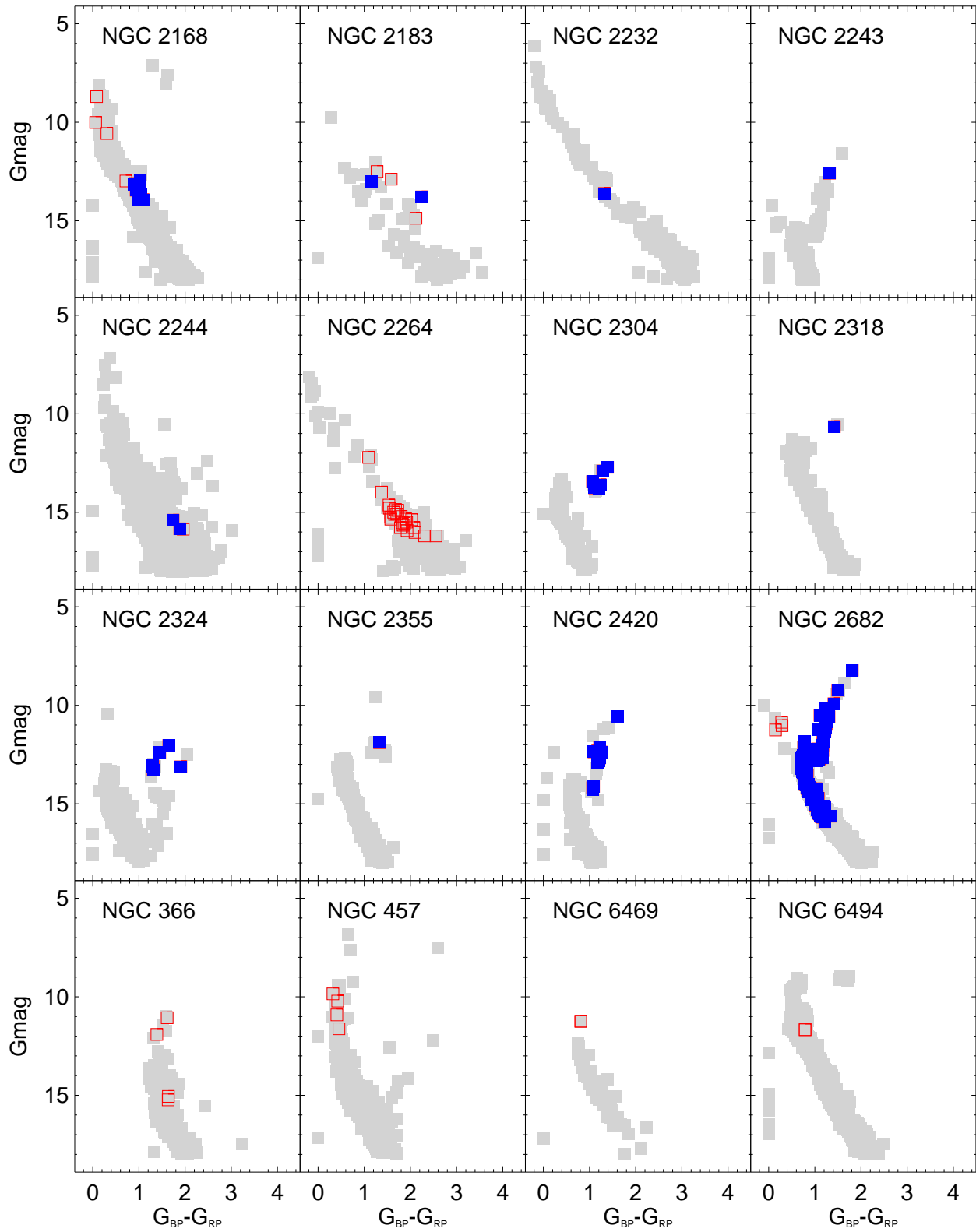


Fig. A.1. continued.

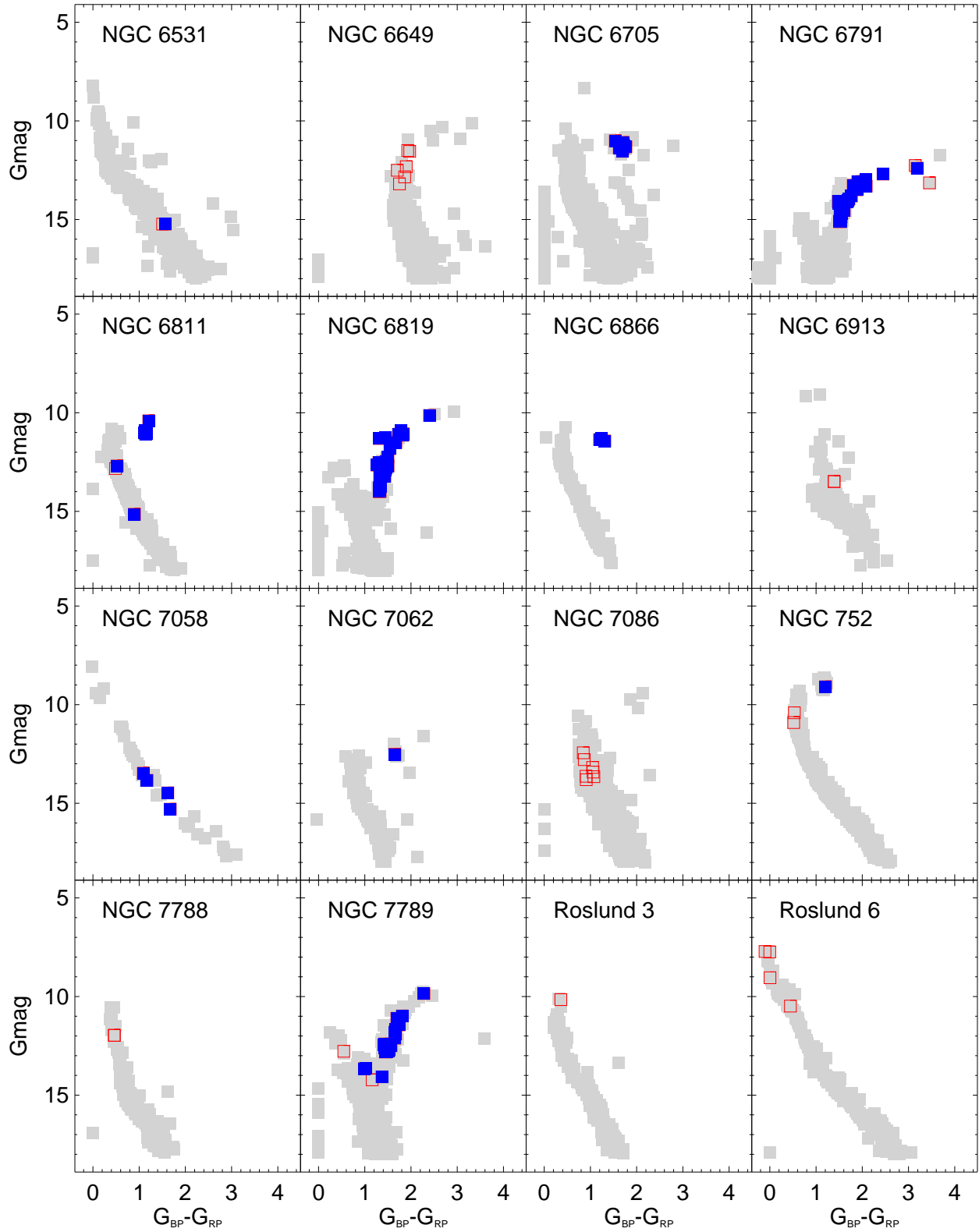


Fig. A.1. continued.

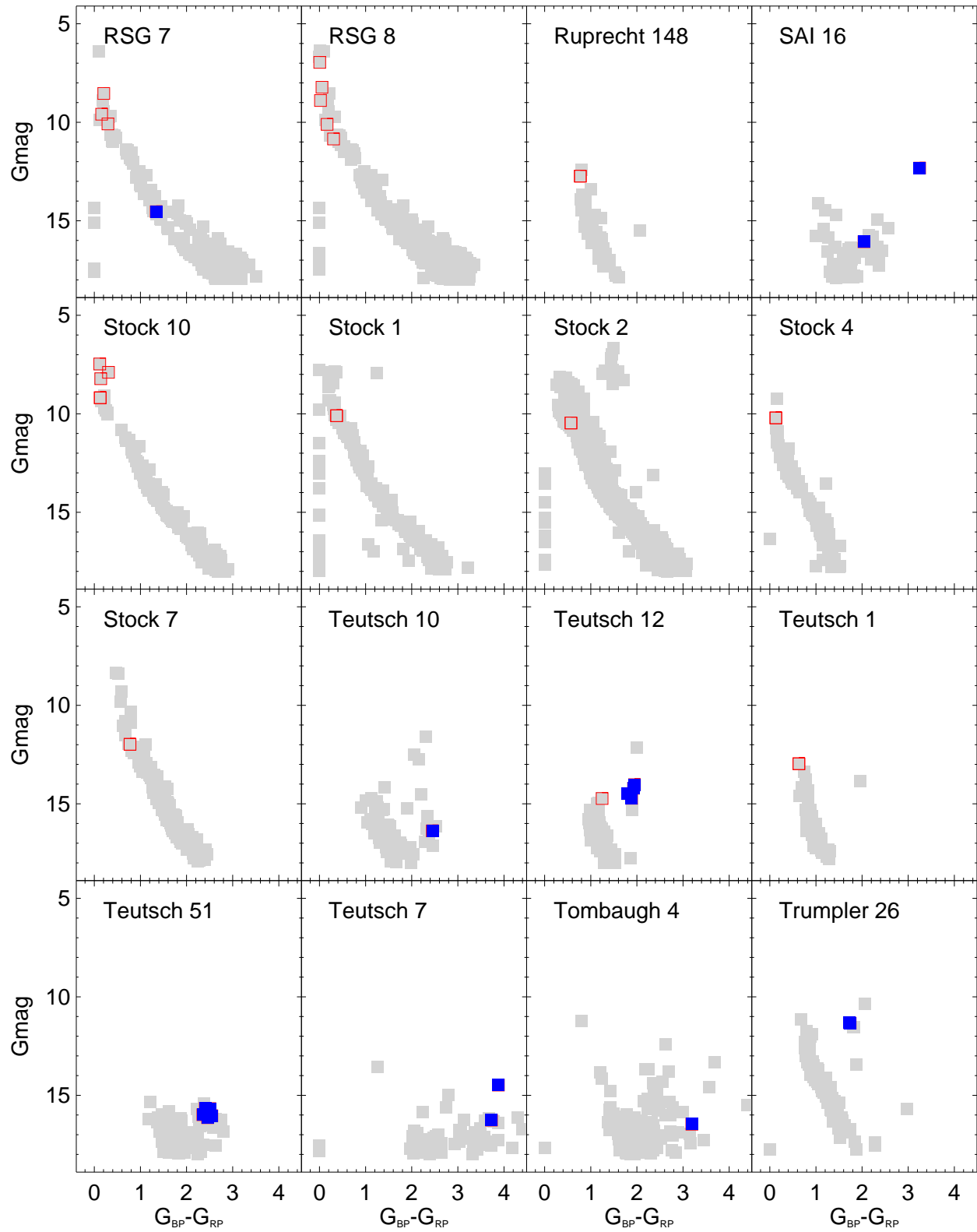


Fig. A.1. continued.

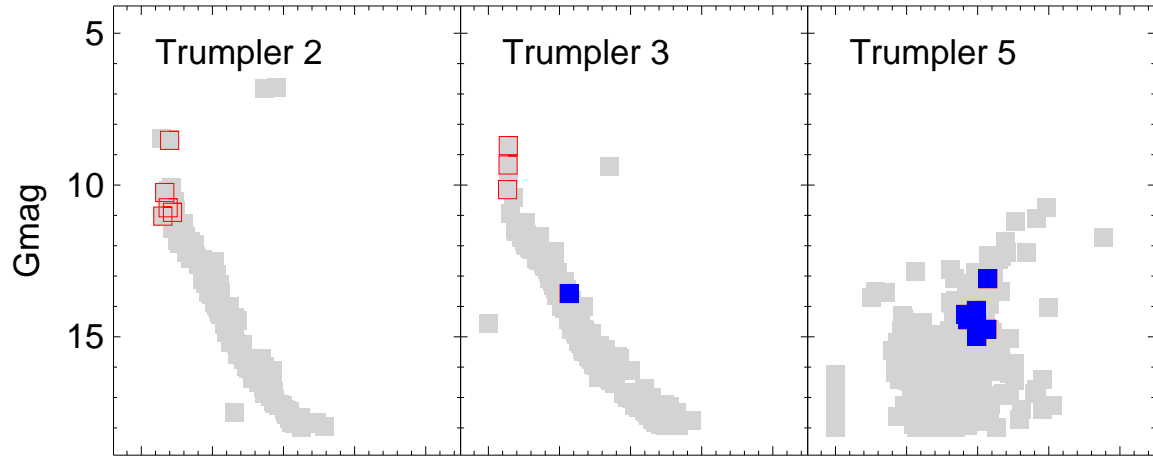


Fig. A.1. continued.